

Formation of Archean batholith-hosted gold veins at the Lac Herbin deposit, Val-d'Or district, Canada: Mineralogical and fluid inclusion constraints

Hervé Rezeau¹  · Robert Moritz¹ · Georges Beaudoin²

Received: 4 June 2015 / Accepted: 21 June 2016 / Published online: 16 July 2016
© Springer-Verlag Berlin Heidelberg 2016

Abstract The Lac Herbin deposit consists of a network of mineralized, parallel steep-reverse faults within the synvolcanic Bourlamaque granodiorite batholith at Val-d'Or in the Archean Abitibi greenstone belt. There are two related quartz-tourmaline-carbonate fault-fill vein sets in the faults, which consist of subvertical fault-fill veins associated with subhorizontal veins. The paragenetic sequence is characterized by a main vein filling ore stage including quartz, tourmaline, carbonate, and pyrite-hosted gold, chalcopyrite, tellurides, pyrrhotite, and cubanite inclusions. Most of the gold is located in fractures in deformed pyrite and quartz in equilibrium with chalcopyrite and carbonates, with local pyrrhotite, sphalerite, galena, cobaltite, pyrite, or tellurides. Petrography and microthermometry on quartz from the main vein filling ore stage reveal the presence of three unrelated fluid inclusion types: (1) gold-bearing aqueous-carbonic inclusions arranged in three-dimensional intragranular clusters in quartz crystals responsible for the main vein filling stage, (2) barren high-temperature, aqueous, moderately saline inclusions observed in healed fractures, postdating the aqueous-carbonic inclusions, and considered as a remobilizing agent of earlier precipitated gold in late fractures, and (3) barren low-

temperature, aqueous, high saline inclusions in healed fractures, similar to the crustal brines reported throughout the Canadian Shield and considered to be unrelated to the gold mineralization. At the Lac Herbin deposit, the aqueous-carbonic inclusions are interpreted to have formed first and to represent the gold-bearing fluid, which were generated contemporaneous with regional greenschist facies metamorphism. In contrast, the high-temperature aqueous fluid dissolved gold from the main vein filling ore stage transported and reprecipitated it in late fractures during a subsequent local thermalevent.

Introduction

The Superior craton in Canada contains 39 % of the global Archean lode gold endowment, if paleoplacers are not considered (Mercier-Langevin et al. 2012). Most of the gold comes from the Archean Abitibi greenstone belt (e.g., Robert et al. 2005; Dubé and Gosselin 2007; Lydon 2007), which is the largest and best-preserved supracrustal sequence in the Superior craton, Canada (Card 1990).

The Val-d'Or mining district is located in the southeastern Abitibi subprovince and hosts classic examples of orogenic gold deposits along main regional faults and in subsidiary second- and third-order faults (Fig. 1). Two gold mineralization events are reported in the Val-d'Or mining district, one predating 2692–2686 Ma, and one younger than 2682 ± 2 Ma (e.g., Feng et al. 1992; Kerrich and King 1993; Robert et al. 2005). The Val-d'Or district is also the site for some of the pioneering investigations on fluids associated with orogenic gold deposits. Fluid inclusion studies were typically focused on auriferous veins from gold deposits hosted by volcanic rocks (Robert and Kelly 1987; Chi et al. 1992; Robert et al. 1995; Firdaous 1995; Boullier et al. 1998; Olivo and

Editorial handling: S. Hagemann

Electronic supplementary material The online version of this article (doi:10.1007/s00126-016-0669-5) contains supplementary material, which is available to authorized users.

✉ Hervé Rezeau
herve.rezeau@unige.ch

¹ Department of Earth Sciences, University of Geneva, rue des Maraîchers 13, CH-1205 Geneva, Switzerland

² Département de Géologie et de Génie Géologique, Université Laval, avenue de la Médecine 1065, Québec, QC, Canada G1V 0A6

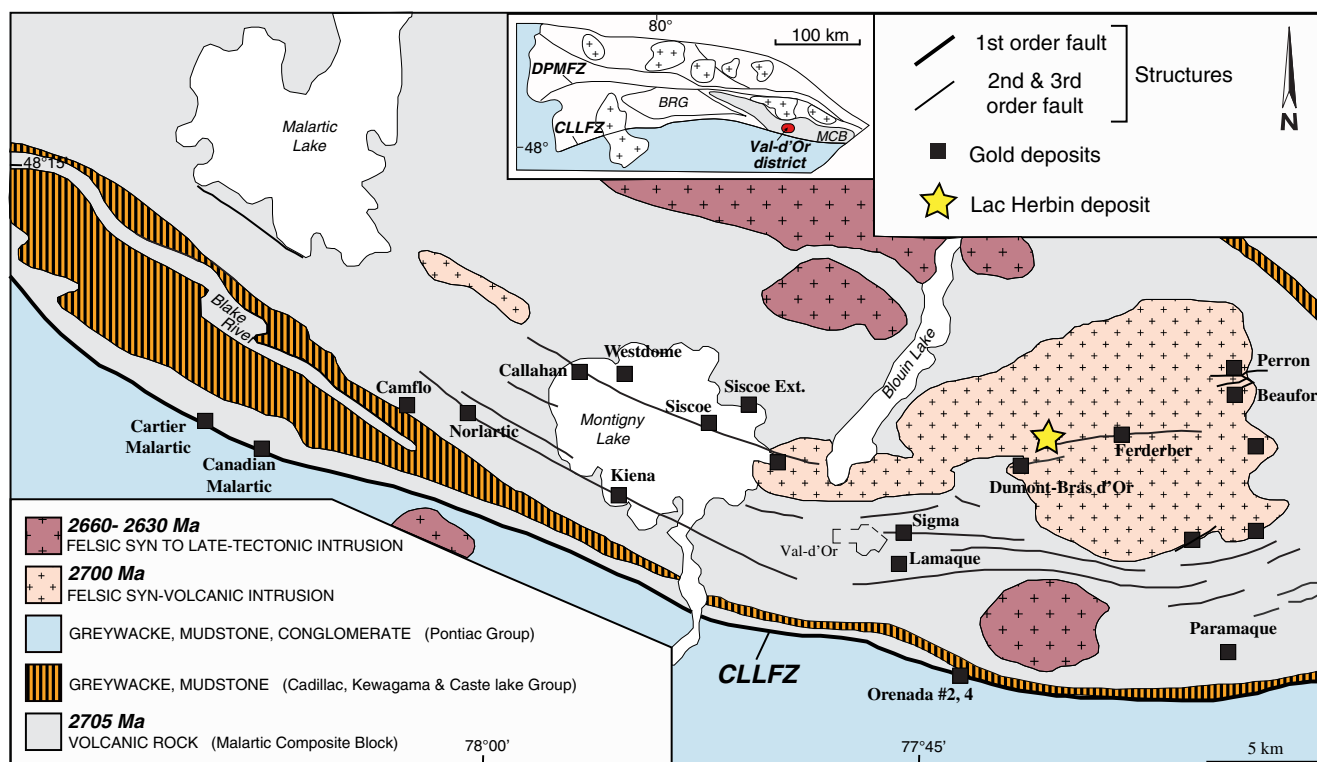


Fig. 1 Geology of the Val-d'Or mining district, including location of first-, second-, and third-order faults, the Cadillac-Larder-Lake fault zone (CLLFZ), and selected gold deposits. *Inset* shows the location of the transcrustal fault zones in the Abitibi province, the Malartic Composite

Block (MCB), and the Black River Group (BRG). *DPMFZ* Destor-Porcupine-Manneville fault zone. Modified after Neumayr and Hagemann (2002)

Williams-Jones 2002; Neumayr and Hagemann 2002; Olivo et al. 2006; Neumayr et al. 2007). These investigations reported CO_2 -bearing, and low- to high-temperature aqueous fluids with different salinities. The CO_2 -bearing, low-salinity fluid, within a temperature range of 250–350 °C is generally considered as the ore-forming fluid. Nevertheless, open questions remain about the main processes responsible for ore deposition, such as fluid immiscibility vs fluid mixing (e.g., Sigma mine: Robert et al. 1995 vs Olivo et al. 2006), and the relationship of high-temperature, saline aqueous fluids with the ore forming events (e.g., Boullier et al. 1998; Olivo et al. 2006 vs Neumayr et al. 2007). In addition, the timing of gold introduction with respect to the succession of thermal events remains a matter of debate, partly related to the lack of evidence for primary and pseudo-secondary fluid inclusion characteristics in the previous studies.

We carried out the first fluid inclusion study on a gold vein system at the Lac Herbin deposit in the Val-d'Or mining district (Fig. 1). In contrast to most of the previous fluid inclusion studies, which mainly focused on veins hosted by volcanic rocks, the mineralized veins are hosted by the granodioritic Bourlamaque batholith. In this study, we report about a detailed paragenetic sequence of ore-forming hydrothermal events including eight new tellurides species for the Val-d'Or mining district and combine detailed petrography,

microthermometry, and Raman spectroscopy of fluid inclusions hosted in quartz, to characterize fluid compositions, and pressure and temperature conditions. We use the mineral paragenesis and fluid inclusion data to constrain the timing and conditions of each hydrothermal fluid event and their respective link with the ore mineralogy. Finally, we offer a new interpretation for the high-temperature, moderate salinity aqueous fluid recognized previously, and discuss its role as a remobilizing agent of earlier precipitated gold into late fractures.

Regional geological setting and gold mineralization

The Archean Abitibi subprovince constitutes a segment of a broad volcanic arc constructed during three major periods of volcanism at 2730–2725, 2718–2714, and 2705–2700 Ma (Corfu et al. 1989; Chown et al. 2002). Each volcanic cycle has a basal komatiitic unit, overlain by tholeiitic basalts, calc-alkaline, and locally alkaline felsic volcanic rocks, and associated metasedimentary rocks (Dimroth et al. 1982; Jensen and Langford 1985; Ayer et al. 2002). North-south shortening produced thrusts and folds between 2700 and 2692 Ma, resulting in the accretion of tectono-magmatic zones along the regional crustal-scale Destor-Porcupine-Manneville, and the Cadillac-Larder-Lake dextral strike-slip fault zones

(Hubert et al. 1984; Ludden et al. 1986; Chown et al. 2002; Daigneault et al. 2002; Fig. 1). Igneous activity started at ca. 2700 Ma with the emplacement of synvolcanic tonalite-trondhjemite-granodiorite series, followed by syntectonic calc-alkaline tonalite-granodiorite-monzodiorite and syn- to late-tectonic subalkaline monzogranite at ca. 2700–2680 and ca. 2690–2670 Ma, respectively (Corfu et al. 1989; Rive et al. 1990; Feng and Kerrich 1992; Feng et al. 1992; Chown et al. 2002). The Abitibi belt was metamorphosed to the greenschist facies at ca. 2690–2670 Ma (Jolly 1978; Dimroth et al. 1983; Ludden et al. 1986; Card 1990; Wong et al. 1991) along with three major phases of deformation (i.e., D1 to D3, see details in Robert 1989, 1990; Desrochers and Hubert 1996; Robert and Poulsen 2001). A post-tectonic, S-type, garnet-muscovite granite was emplaced at ca. 2645–2611 Ma and resulted in contact metamorphism (Feng and Kerrich 1991; Kerrich and King 1993; Chown et al. 2002).

The Val-d'Or mining district is located in the eastern segment of the Southern Volcanic Zone of the Archean Abitibi subprovince along the Cadillac-Larder-Lake fault zone, at the boundary with the Pontiac subprovince (CLLFZ in Fig. 1). This fault zone dips to the north and is a reverse shear zone spatially associated with numerous gold deposits and occurrences (Robert 1989, 1994; Robert et al. 2005). The host rocks of the Val-d'Or mining district belong to the volcano-sedimentary sequences of the Malartic Group and the Louvicourt Group, intruded by calc-alkaline plutonic rocks (Fig. 1). The Malartic Group comprises mainly komatiitic and tholeiitic basalt flows and sills, with minor sedimentary rocks, which are interpreted as an oceanic floor in an extensional environment related to mantle plumes, whereas the Louvicourt Group is mainly composed of mafic to felsic volcanic rocks that formed in a subduction-related arc setting (Desrochers et al. 1993; Daigneault et al. 2002; Scott et al. 2002).

Two major auriferous events have been recognized in the Val-d'Or mining district on the basis of structural and hydrothermal features (Robert 1994), supported by crosscutting relationships and isotope dating (Couture et al. 1994). Early gold-bearing quartz-carbonate (QC) veins are commonly affected by deformation and crosscut by diorite and tonalite dikes dated at 2692 ± 2 Ma (U-Pb titanite age, Couture et al. 1994) and 2686 ± 2 Ma (U-Pb zircon age, Morasse 1998). Late gold-bearing quartz-tourmaline-carbonate (QTC) veins are characterized by banded, subvertical fault-fill veins associated with subhorizontal veins crosscutting tonalite dikes, which have U-Pb zircon and titanite ages of 2685 ± 3 and 2682 ± 2 Ma, respectively (Lamaque deposit, Fig. 1; Jemielita et al. 1990). Based on these data, the maximum age of the second gold mineralization event associated with the QTC veins is considered to be 2682 ± 2 Ma. However, it is still debated if the second ore-forming fluid was coeval with syn- to late- regional metamorphism at ca. 2682 ± 8 Ma (Claoué-Long et al. 1990; Kerrich and King 1993; Kerrich

and Kyser 1994) or was a postregional metamorphic event, as young as 2600 Ma (Jemielita et al. 1990; Wong et al. 1991; Hanes et al. 1992; Zweng and Mortensen 1993; Anglin et al. 1996; Olivo et al. 2007; Lemarchand et al. 2010; Lemarchand 2012).

The Lac Herbin deposit

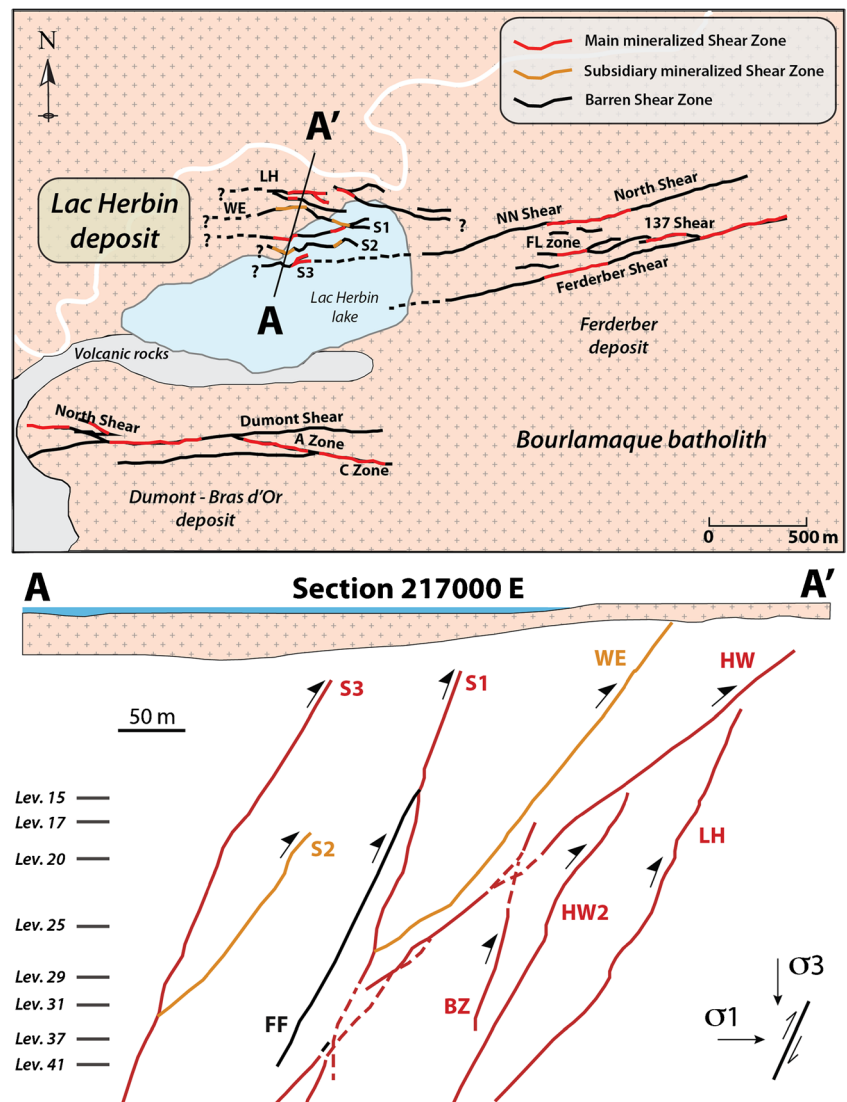
The Bourlamaque batholith

The Bourlamaque batholith has an ovoid shape with the longest axis parallel to the regional structural E-W trend (Jébrak et al. 1991; Fig. 1). It was dated at 2699 ± 1 Ma using U-Pb zircon dating (Wong et al. 1991) and emplaced at 1 kbar (Feng and Kerrich 1992). The batholith is composed of quartz diorite according to their normative feldspar content (Campiglio 1977); however, Jébrak et al. (1991) reclassified it as a diorite-tonalite-granodiorite according to the multicationic classification plot of De La Roche et al. (1980). Surrounding mafic volcanic rocks are intruded by felsic apophyses, and the batholith contains mafic enclaves. The batholith is considered to be synvolcanic and co-magmatic with the Val-d'Or Formation (Latulippe 1966; Campiglio 1977; Imreh 1984; Tanner and Trudel 1989). The Bourlamaque batholith underwent deformation during the D2 event associated with regional greenschist metamorphism (Goulet 1978; Dimroth et al. 1983). The D2-related shear zones in the batholith dip between 35° and 80° to the north and to the south (Belkibir et al. 1993) and host a complex anastomosing vein network with discontinuously mineralized shear segments (Fig. 2). Dioritic porphyritic and aplitic dikes crosscut the batholith (Campiglio 1977; Lemarchand 2012).

Structural and textural setting of the veins

The Lac Herbin deposit consists of 13 shear zones ranging from less than 1 to 3.5 m in width. The mineralized network is composed of six main E-W trending reverse shear zones steeply dipping to the south (LH, HW2, BZ, HW, S1, and S3 in Fig. 2). The main shear zones are the result of the D2 regional deformation, and hydrothermal fluids used these structures as a fluid path. Gold mineralization is associated with banded veins emplaced within these shear zones parallel or at low angle to the shear zone foliation. Two subsidiary mineralized reverse shear zones, S2 and WE, are merging with the main mineralized veins with a NW-SE trend, and they were formed as the result of hydrothermal activity (Fig. 2; Lemarchand et al. 2010). These two subsidiary structures are only mineralized at the junction with the main mineralized structures S3 and S1, respectively. The mineralized shear zones crosscut mafic and felsic dikes (Lemarchand 2012). A network of postmineralization, barren, and brittle faults (FF in Fig. 2)

Fig. 2 Zoom on the batholith-hosted Lac Herbin study area, illustrating the irregular shape of the E-W oriented discontinuous mineralized shear zones. The A-A' cross section shows the structural setting of the Lac Herbin deposit. From QMX Gold Corporation



is located subparallel to the mineralized zones, or they crosscut the latter with an offset of less than 10 cm (Lemarchand 2012).

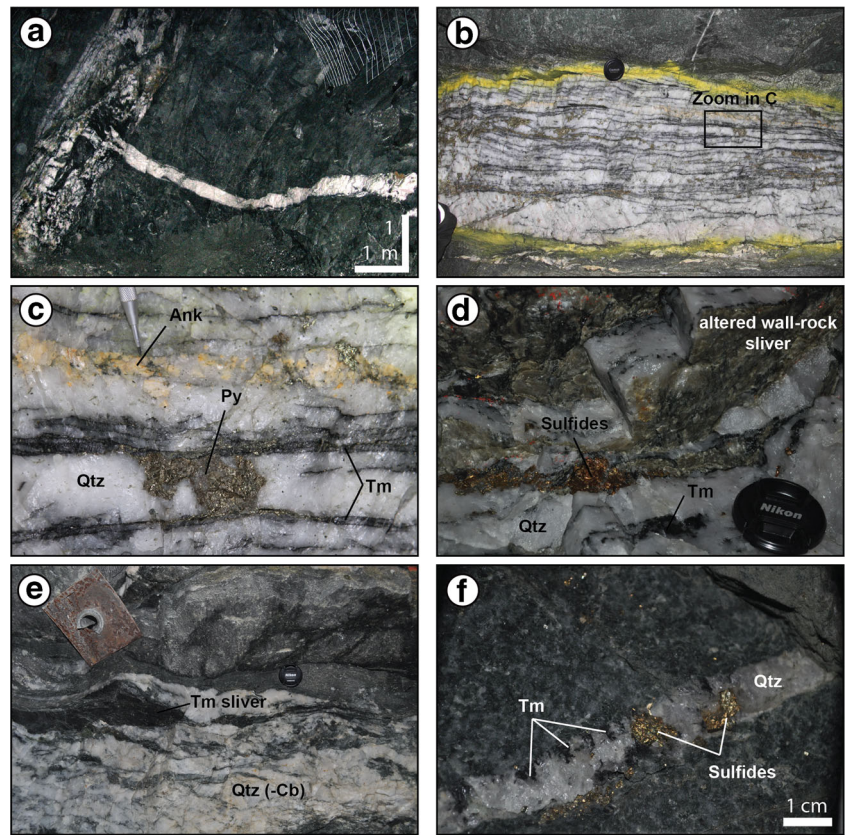
Subvertical fault-fill QTC veins are by far the most voluminous at the Lac Herbin deposit, and they are consistently associated with extension veins (Fig. 3a). Fault-fill veins typically have a banded texture where individual quartz ribbons are separated by slivers of foliated and sericitized wall rock, and by slip surfaces marked by tourmaline (Figs. 3b–e). The incorporation of wall rock slivers is generally considered to be a natural consequence of incremental vein growth (Robert and Brown 1986a, b; Moritz and Crocket 1990; Robert and Poulsen 2001).

Extension veins are contemporaneous with the main fault-fill veins under a compressional regime with a N-S to SW-NE direction (Lemarchand et al. 2010), and their thickness ranges from few centimeters up to a meter. They are at high angle to the wall rock foliation and extend up to several tens of meters

away from the shear zones hosting the fault-fill veins (Fig. 3a). Extension veins are characterized by open-space filling textures with radiating aggregates of tourmaline, and euhedral quartz, carbonate, and pyrite at the vein wall that grew progressively as the fracture opened (Fig. 3f).

At the Lac Herbin deposit, proximal to distal hydrothermal alteration is developed parallel to the vein and consists of, alternating carbonate, white mica and chlorite ribbons, and a groundmass of albite, chlorite, and white mica replacing plagioclase (Fig. 4a). At the Beaufor mine hosted by the Bourlamaque batholith (Fig. 1), Tessier (1990) and Roussy (2003) described wall rock alteration with a bleached inner zone consisting of carbonate-sericite-albite, with a progressive change to an outer zone composed of hydrothermal chlorite together with igneous plagioclase. At the Sigma mine, Robert and Brown (1986b) and Garofalo (2004a, b) reported similar observations for volcanic host-rock alteration patterns.

Fig. 3 **a** Contemporaneous fault-fill and extensional veins. S3 zone - Level 29. **b** Typical fault-fill vein with parallel quartz and tourmaline ribbons, and subsidiary sulfide and carbonates. HW2 zone - Sublevel 25. **c** Detail of **b**. **d** Slivers of foliated and sericitized wall rock. Some oxydized sulfides and tourmaline are also present. HW zone - Sublevel 17. **e** Tourmaline slip-surface. HW zone - Level 25. **f** Extensional vein with a typical open-space filling texture. HW zone - Level 25. *Ank* ankerite, *Py* pyrite, *Tm* tourmaline, *Qtz* quartz



Vein mineralogy

Quartz is the main vein-filling constituent (80 vol%) and commonly contains inclusions of tourmaline and pyrite (Figs. 3b–d, f and 4b, g–h), illustrating continuous deposition of quartz, tourmaline, and pyrite (Robert and Brown 1986b). In fault-fill veins, quartz is typically white and associated with tourmaline ribbons (Figs. 3b–e), which indicate that quartz and tourmaline crystals experienced non-coaxial deformation. Deformed quartz has recrystallization textures with 120° between grain boundaries, sub-grains formation, and undulose extinction. Grey quartz is only found in pressure shadows around pyrite. In extension veins, quartz is typically translucent to grey and associated with tourmaline needles (Fig. 3f), which indicates that it has been weakly deformed. Quartz has a mostly homogeneous, even grey appearance, and cathodoluminescence images rarely reveal growth zones (Fig. 4c). We observed only one quartz generation, which belongs to the main-vein filling ore stage.

Tourmaline fillings occupy an average volume of 10 to 20 vol%, with locally up to 80 vol%. In fault-fill veins, tourmaline typically forms parallel ribbons along slip surfaces (Fig. 3b–e). In extension veins, fibrous tourmaline is perpendicular to oblique to the vein walls (Fig. 3f). Tourmaline needles form inclusions in quartz and pyrite (Fig. 4b, d). Tourmaline typically consists of a blue-green core with brown rims under transmitted light (Fig. 4e). Tourmaline is mainly

dravitic, ranging in composition from Ca-poor, higher X-site vacancy tourmaline, toward Ca-rich and dominantly sodic tourmaline (Beaudoin et al. 2013).

Chlorite occurs as a green groundmass or as radiating aggregates surrounding tourmaline and interstitial to recrystallized quartz (Fig. 4e). Chlorite has a strong green to light brown bireflectance and has the composition of ripidolite (Robert and Brown 1986b; Roussy 2003). Hydrothermal chlorite in veins and wall rock has similar compositions (Roussy 2003).

White mica is present in the wall rock alteration and in veins, but its temporal relationship with other hydrothermal minerals remains uncertain. In the Val-d’Or district, white mica ranges in composition from phengite to sericite (Robert and Brown 1986b; Roussy 2003).

Carbonates with an average volume of 5 vol%, and locally up to 25 vol% in veins, range in composition from calcite (CaCO₃) to ankerite (Ca(Fe,Mg,Mn)(CO₃)₂). The first generation of carbonate is characterized by euhedral crystals up to one centimeter in size, forming a ribbon at the selvage of the veins (Fig. 4b). The early carbonate contains growth zones and inclusions of gold (Fig. 4f). A second generation of carbonate surrounds and fills fractures in quartz, pyrite, and tourmaline. It is associated with gold and chalcopyrite, and locally with pyrrhotite, sphalerite, cobaltite, galena, pyrite, or tellurides (Figs. 4i, j).

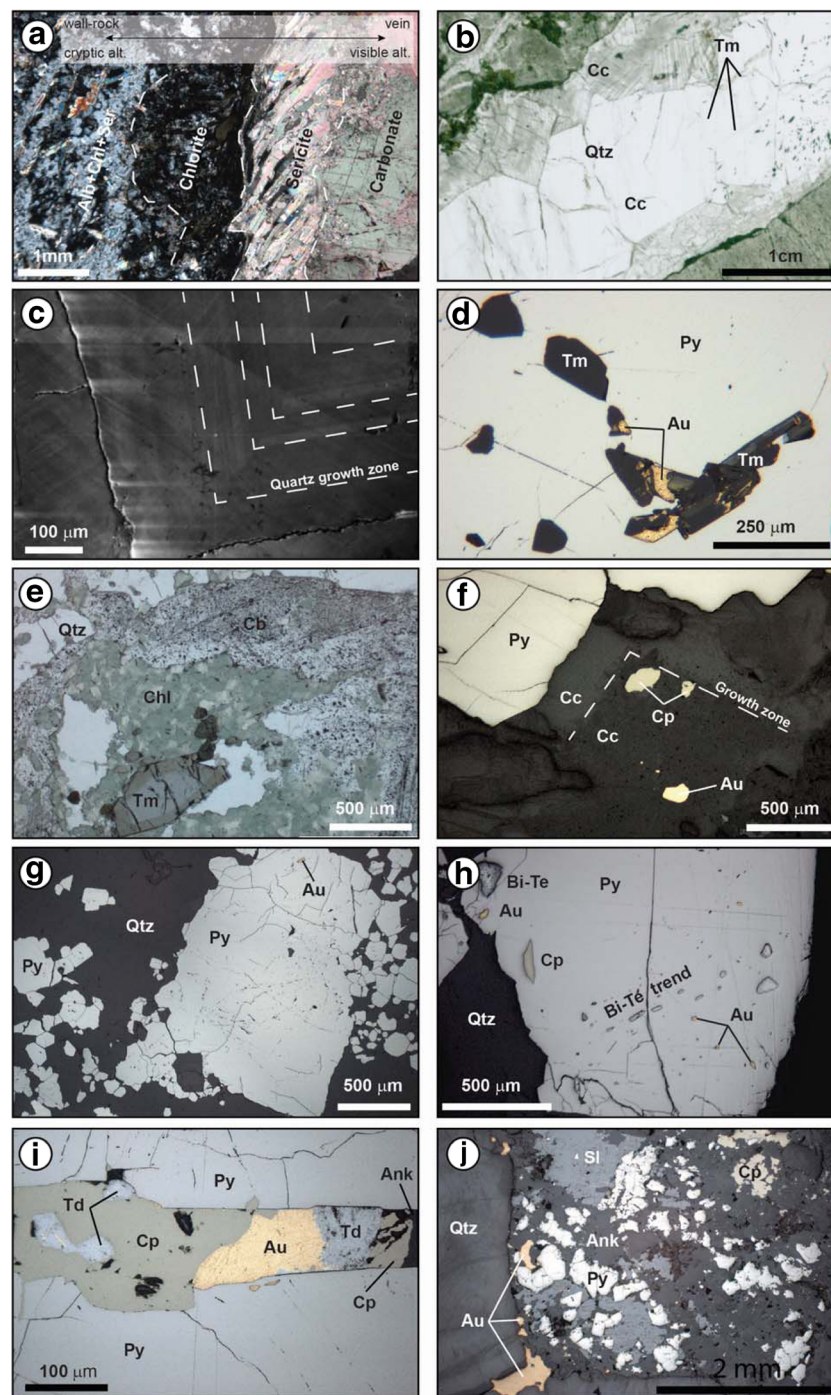


Fig. 4 **a** Proximal to distal hydrothermal alteration sequence from the vein into the wall-rock. AM39956 - HW zone - 50 m. **b** Vein of the main filling stage with carbonate along the selvage, and tourmaline needles within quartz in the central part of the vein. AM58901 - LH zone - N25. **c** Cathodoluminescence image showing growth zones in quartz crystal of the main filling stage. AM58902 - LH zone - N25. **d** Tourmaline-gold inclusions in pyrite of the main filling stage. AM58906 - between BZ and HW zone - N29. **e** Main quartz filling stage with zoned tourmaline (blue to brown from core to rim) surrounded by chlorite and interstitial carbonate. AM58908 - between BZ and HW zone - N29. **f** Gold and chalcopyrite inclusions in the first generation of carbonates. AM39928 - S1 zone - 380 m. **g** Gold-bearing pyrite with a

cataclastic texture. AM58906 - between BZ and HW zone - N29. **h** Inclusions of chalcopyrite, tellurides, and gold in pyrite. AM58906 - between BZ and HW zone - N29. **i** Pyrite fracture filled by chalcopyrite-gold-telluride associated with the second generation of carbonates. AM39914 - HW2 zone - 50 m. **j** Gold, sphalerite, chalcopyrite, pyrite, and the second generation of carbonates crosscutting quartz of the main filling stage. AM39984 - between S3 and S1 zone - 180 m. *Au* gold, *Ank* ankerite, *Bi-Te* bismuth-tellurides, *Cb* carbonate, *Cal* calcite, *Chl* chlorite, *Cp* chalcopyrite, *Py* pyrite, *Qtz* quartz, *Sl* sphalerite, *Td* tetradymite, *Tm* tourmaline. Ore minerals are abbreviated according to Chace (1956), and gangue minerals according to Kretz (1983)

Pyrite is the dominant sulfide in both fault-fill and extension vein types, forming euhedral to sub-euhedral crystals with a grain size of millimeters up to few centimeters. Pyrite is disseminated in altered wall rocks, or intergrown with quartz in veins (Figs. 3b–d, f and 4g–h). Pyrite contains inclusions of tourmaline, chalcopyrite, pyrrhotite, gold, tellurides, and cubanite (Fig. 4d, g–h) and has been variably affected by brittle deformation (Fig. 4g). Rare pyrite associated with the second generation of carbonates, gold, chalcopyrite, and sphalerite is interstitial to quartz (Fig. 4j). Pyrite consists of concentric Co- and As-rich growth zones (ESM 1: Tables S1 and S2), which are associated with gold, chalcopyrite, and tellurides inclusions. At the Beaufort mine, Roussy (2003) reported that Co-rich pyrite is associated with gold, chalcopyrite, and telluride inclusions.

Chalcopyrite forms irregular millimeter to centimeter grains or aggregates. Early chalcopyrite forms inclusions in pyrite, either isolated or in equilibrium with gold, pyrrhotite, tellurides, and cubanite (Fig. 4h). It was also observed in the first generation of carbonate associated with gold (Fig. 4g). Late chalcopyrite fills fractures in pyrite, tourmaline, and quartz in close association with the second generation of carbonate, gold, sulfides, and tellurides (Figs. 4i, j).

Pyrrhotite forms rare inclusions in pyrite in association with chalcopyrite. It also fills fractures in pyrite associated with the second generation of carbonate, chalcopyrite, sphalerite, cobaltite, and galena. Pyrrhotite contains rare flame-like exsolutions of pentlandite.

Sphalerite and rare galena are associated with the second generation of carbonates, chalcopyrite, pyrrhotite, cobaltite, galena, and gold, filling fractures in pyrite, tourmaline, and quartz (Fig. 4j).

Cobaltite forms euhedral crystals in pyrrhotite or fills fractures in pyrite, carbonate, and tourmaline associated with sphalerite and chalcopyrite. The cobaltite chemistry is reported in ESM 1: Table S1.

Cubanite forms rare micrometer inclusions in pyrite and is locally associated with chalcopyrite or telluride inclusions.

Ilmenite and rutile are observed within chlorite and also as inclusions in pyrite.

Native gold forms isolated grains with electrum rims in equilibrium with chalcopyrite, Bi-, Au-, Ag-, and Ni-tellurides inclusions in pyrite, tourmaline, and the first generation of carbonate (Figs. 4d, f–h and 5a, c, e, f). Most of the gold, however, is associated with the second generation of carbonate, sulfides, and tellurides, filling fractures in pyrite (Fig. 4i) and quartz (Fig. 4j). The Au/Ag ratio of native gold ranges between 95:5 and 85:15, whereas the Au/Ag ratio of electrum rimming gold grains ranges between 70:30 and 80:20 (ESM 1: Table S3).

Tellurides form isolated inclusions in pyrite and fill fractures in pyrite and quartz (Figs. 5a–f). Among 11 recognized

Au-, Ag-, Bi-, Pb-, Ni-, and S-bearing tellurides (ESM 1: Table S4), only three of them have never been observed associated with gold, they are hessite, stützite, and volynskite. There is no systematic correlation between telluride composition and the presence of gold (Fig. 6).

Parkerite, a Ni-bearing bismuth sulfide phase, is also observed (Fig. 6 and ESM 1: Table S4).

Vein paragenetic sequence

The paragenetic sequence for subvertical fault-fill and subhorizontal extensional veins (Fig. 7) is similar to that described by Robert and Brown (1986b) at the Sigma mine and by Roussy (2003) at the Beaufort mine. At the Lac Herbin deposit, mineralization is divided into two events: a main vein-filling event and a fracture-filling event.

The main vein-filling event is characterized by the deposition of a first generation of carbonate, precipitated along the selvages of the veins, followed by abundant quartz and tourmaline. Tourmaline forms within and surrounds disseminated pyrite crystals indicating that deposition of both minerals is coeval. Pyrite contains inclusions of gold, pyrrhotite, chalcopyrite, cubanite, and a variety of tellurides. This early mineralizing event underwent deformation illustrated by pyrite with cataclastic textures. The fracture-filling event cements fractures in pyrite and quartz and includes the second generation of carbonate, in equilibrium with gold and chalcopyrite, and local association of sphalerite, pyrrhotite, cobaltite, galena, pyrite, or tellurides. Tellurides are never observed in equilibrium with sphalerite, pyrrhotite, cobaltite, and galena. Chlorite is considered to have precipitated late in the hydrothermal veins, during a reopening of the second generation of carbonate. Ilmenite and rutile exsolutions are only observed where chlorite is located, and therefore, they are interpreted as coeval or postdating chlorite.

Analytical methods

Thirty-nine doubly-polished thick sections were examined under the petrographic microscope to select fluid inclusion assemblages (FIAs; Goldstein and Reynolds 1994); of these, seven contained FIAs adequate to carry out microthermometry. We selected FIAs avoiding inclusions showing evidence not only of “necking-down” or shape modifications but also on the mode of occurrence, such as clusters, alignment along growth zone, or crosscutting grain boundaries. Cathodoluminescence imaging using a scanning electron microscope (SEM-CL) was carried out to reveal growth zones in order to characterize the “primary,” “pseudo-secondary,” and “secondary” character of the fluid inclusion types. However, quartz remains predominantly non-luminescent under SEM-CL, and no fluid inclusions were observed along the rare quartz growth zones revealed by SEM-CL (Fig. 4c). Infrared (IR) microscopy was

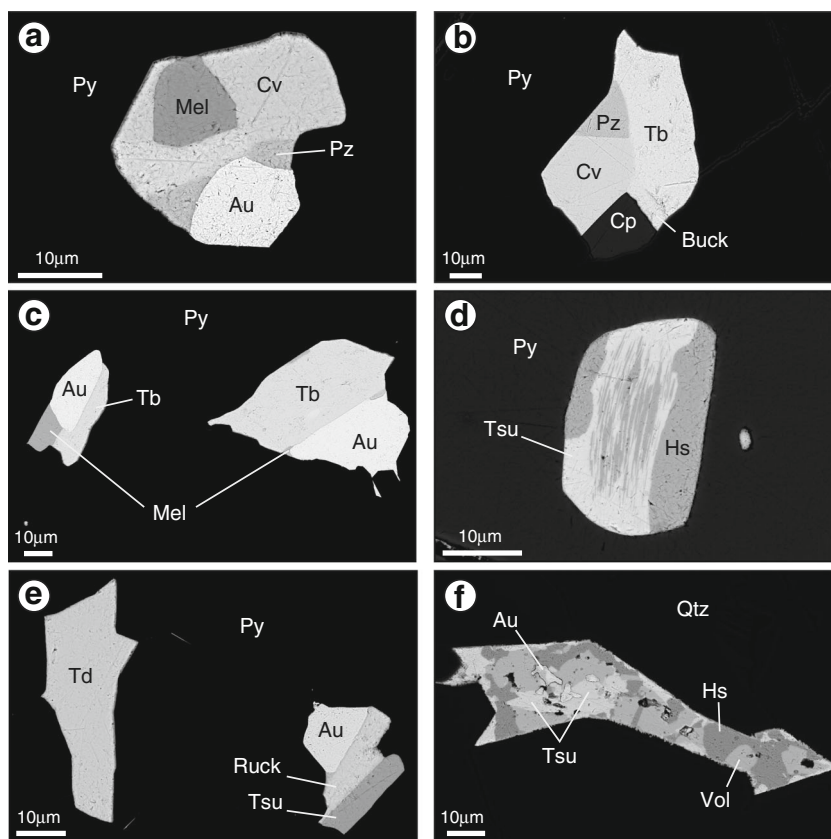


Fig. 5 **a** Melonite-calaverite-petzite-gold assemblage as inclusion in pyrite of the first filling stage. AM39918 - HW zone - N25. **b** Petzite-calaverite-tellurobismuthite-buckhornite-chalcopyrite assemblage as inclusion in pyrite of the first filling stage. AM39918 - HW zone - N25. **c** Melonite-tellurobismuthite-gold inclusions hosted by pyrite of the first filling stage. AM39918 - HW zone - N25. **d** Exsolution of hessite in tsumoite inclusion hosted by pyrite. AM58906 - between BZ and HW zone - N29. **e** Tetradymite and tsumoite-rucklidgeite-gold inclusions

hosted by pyrite. AM58906 - between BZ and HW zone - N29. **f** Exsolution texture consisting of a volynskite-hessite-tsumoite-gold assemblage hosted by quartz. AM58906 - between BZ and HW zone - N29. *Au* gold, *Buck* buckhornite, *Cp* chalcopyrite, *Cv* calaverite, *Hs* hessite, *Mel* melonite, *Py* pyrite, *Pz* petzite, *Qtz* quartz, *Ruck* rucklidgeite, *Tb* tellurobismuthite, *Td* tetradymite, *Tsu* tsumoite, *Vol* volynskite. Ore minerals are abbreviated according to Chace (1956), and gangue minerals according to Kretz (1983)

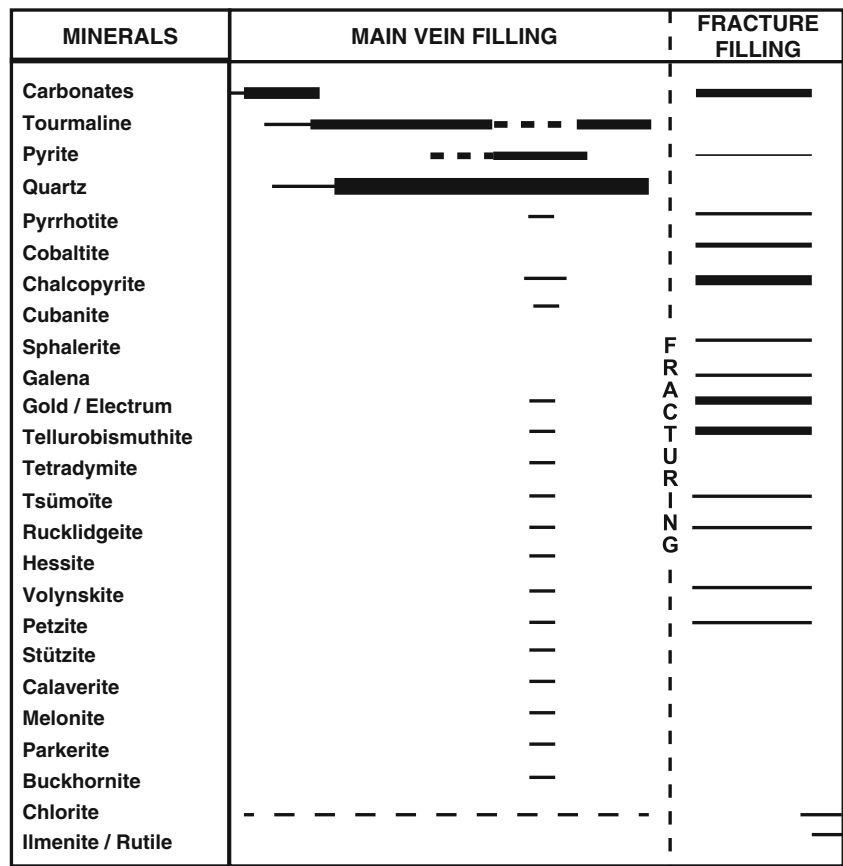
used to identify fluid inclusions in pyrite, but since Lac Herbin pyrite contains Co, Ni, and As, it remained opaque under IR (see Kouzmanov et al. 2002). Fluid inclusions in sphalerite appeared

dark due to internal reflections, which prevented petrographic observations and microthermometry. Detailed microthermometry results are given in ESM 1: Table S5.

Minerals	Calaverite (AuTe ₂)	Buckhornite (AuTe ₂ Pb ₂ BiS ₃)	Petzite (AgAuTe ₂)	Tsumoite (BiTe)	Tellurobismuthite (Bi ₂ Te ₃)	Rucklidgeite (Bi ₃ Te ₄)	Tetradymite (Bi ₂ Te ₂ S)	Melonite (NiTe ₂)	Hessite (Ag ₂ Te)	Stützite (Ag _{5-x} Te ₃)	Volynskite (AgBiTe ₂)	Parkerite (Ni ₃ Bi ₂ S ₂)
Calaverite (AuTe ₂)		X	X		X			X				
Buckhornite (AuTe ₂ Pb ₂ BiS ₃)	X		X		X			X				
Petzite (AgAuTe ₂)	X	X			X			X				
Tsumoite (BiTe)						X	X		X	X	X	X
Tellurobismuthite (Bi ₂ Te ₃)	X	X	X					X				
Rucklidgeite (Bi ₃ Te ₄)				X								
Tetradymite (Bi ₂ Te ₂ S)				X								
Melonite (NiTe ₂)	X		X		X							
Hessite (Ag ₂ Te)				X							X	
Stützite (Ag _{5-x} Te ₃)				X							X	X
Volynskite (AgBiTe ₂)				X					X	X		X
Parkerite (Ni ₃ Bi ₂ S ₂)				X						X	X	

Fig. 6 Telluride associations based on our microscopy observations. Minerals highlighted in yellow indicate tellurides associated with gold

Fig. 7 Paragenetic sequence recognized at the Lac Herbin deposit. *Line thickness* represents schematically the relative abundance of the precipitated minerals. *Dotted lines* indicate uncertainties. See text for explanations



Microthermometry was carried out using a Linkham heating-freezing stage (THMSG 600) mounted on a DMLB Leica microscope and a Linkham heating-freezing stage (FTIR 600) mounted on a BX51 Olympus microscope. The heating-freezing stages were calibrated using synthetic fluid inclusions (Sterner and Bodnar 1984) at -56.6 , 0.0 , and 374.1 °C. The stage uncertainty is ± 0.1 °C for temperatures below 0 and ± 1 °C for homogenization temperatures. Salinities and densities were calculated using the appropriate equations of state, included in the computer program by Bakker (2003) available on the University of Leoben web site at <http://fluids.unileoben.ac.at/Computer.html>. The presence of CO_2 was determined using Raman microscopy measurements on single fluid inclusions using a Renishaw inVia Reflex equipped with a 633 nm He-Ne laser coupled with a Leica DM2500 microscope, at the Natural History Museum of Geneva. Detection limit for CO_2 using Raman spectroscopy is 0.2 mol% CO_2 (Bodnar et al. 1985).

Fluid inclusion study

Sampling approach

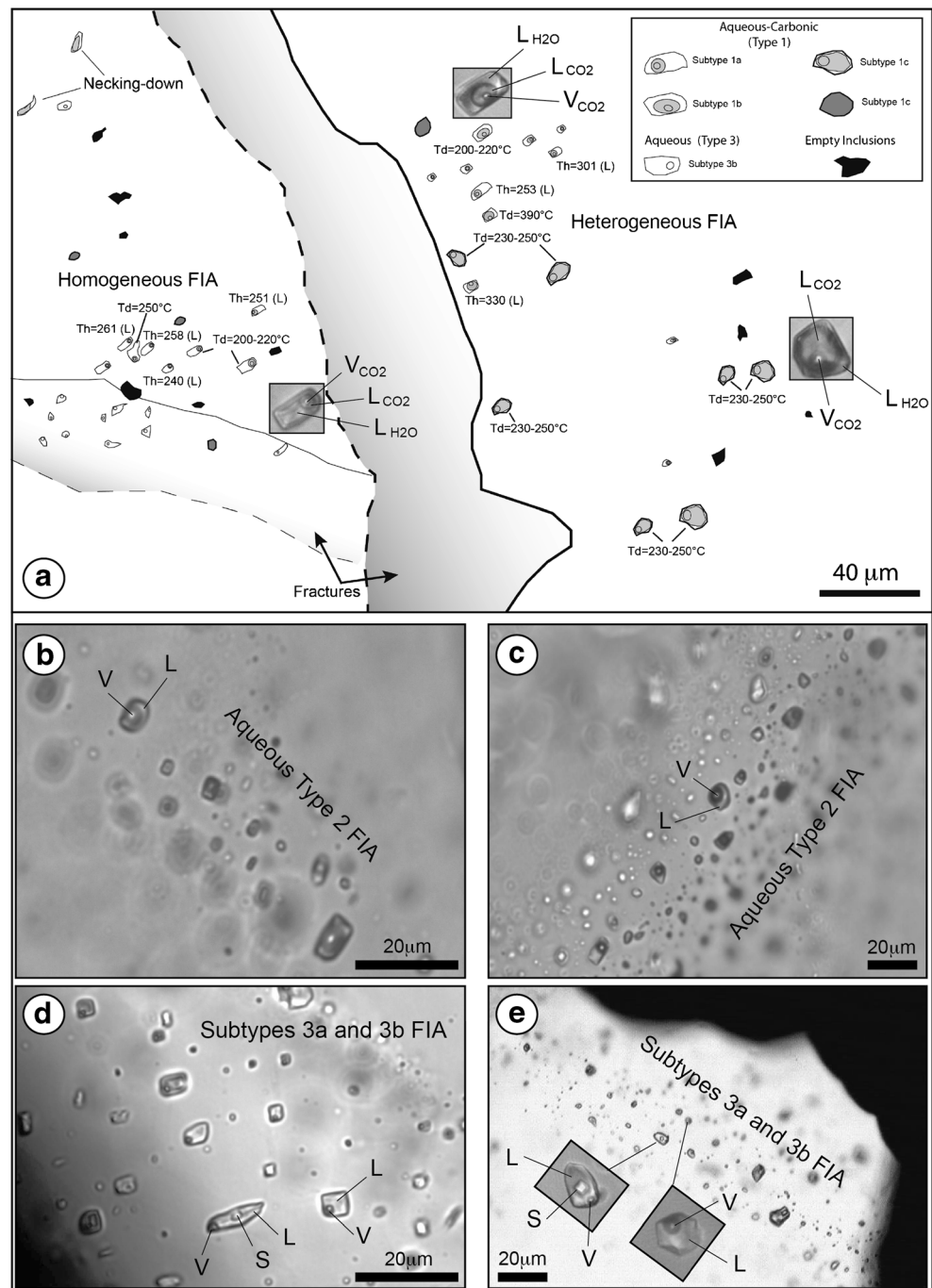
Representative samples were collected underground and from drill-cores from both fault-fill and extensional quartz-tourmaline-carbonate veins. Samples were selected based on

three criteria: (1) grayish to translucent quartz is typically least-deformed compared to the milky quartz (Beaudoin and Pitre 2005), (2) quartz intergrown with undeformed tourmaline needles, and (3) translucent quartz observed in pressure shadow of pyrite. All fluid inclusions of this study and described below were observed in quartz from the main vein-filling stage. Minerals from the fracture-filling stage did either not contain fluid inclusions (e.g., in carbonates) or were not suitable for fluid inclusion petrography and microthermometry (e.g., sphalerite).

Types of fluid inclusions

Type 1 are rare aqueous-carbonic fluid inclusions ranging from 5 to 15 μm in size with a rounded, sub-rectangular, and irregular shape (Fig. 8a, Tables 1 and ESM 1: Table S5). They have variable liquid/vapor (L/V) ratios and have been subdivided in three subtypes based on the volume of the vapor phase after CO_2 homogenization. Subtype 1a consists of inclusions with a vapor phase occupying between 10 and 25 vol% of the inclusion, subtype 1b between 40 and 50 vol%, and subtype 1c between 70 and 90 vol% (Fig. 8a, Tables 1 and ESM 1: Table S5). Some inclusions included in subtype 1c are carbonic without a visible aqueous phase, but it is likely that a thin rim of liquid surrounds the large gas bubble. The small amount of liquid did not allow measuring

Fig. 8 **a** Distribution of Types 1 and 3 fluid inclusions hosted in quartz. The numbers indicate the homogenization temperatures to the liquid phase (T_{TOT}) and decrepitation temperature. Pictures show the three subtypes of Type 1 aqueous-carbonic inclusions associated with homogeneous and heterogeneous fluid inclusion assemblages. AM39928 - S1 zone - 380 m. **b** Type 2 fluid inclusion assemblages aligned along healed fractures in quartz. AM39984 - between S3 and S1 zone - 180 m. **c** Type 2 fluid inclusion assemblages aligned along healed fractures in quartz. AM58901 - LH zone - N25. **d** Subtypes 3a and 3b fluid inclusion assemblages hosted by healed fractures in quartz. AM58925 - Junction HW2 and WE - SN25. **e** Subtypes 3a and 3b fluid inclusion assemblages hosted by healed fractures in quartz. AM58901 - LH zone - N25. *L* liquid, *V* vapor, *S* solid daughter crystal (halite)



aqueous liquid phase transitions (Ramboz et al. 1982). Several subtype 1b and 1c inclusions only contain a single CO_2 phase at room temperature. Type 1 inclusions are randomly distributed as intra-granular three-dimensional clusters and form homogeneous (i.e., one subtype) or heterogeneous (i.e., three subtypes) FIAs in quartz (Fig. 8a). They were never observed within healed fractures; therefore, they are interpreted to be the earliest fluid inclusions at the Lac Herbin deposit.

Type 2 refers to aqueous fluid inclusions, which are more abundant than Type 1 inclusions. Their sizes range from 5 to

25 μm in size with a rounded to subrectangular shape (Figs. 8b, c, Tables 1 and ESM 1: Table S5). They contain a vapor phase occupying 15 to 30 vol% of the inclusion volume. Type 2 FIAs are distributed within healed fractures that cross-cut quartz grains boundaries (Figs. 8b, c, Tables 1 and ESM 1: Table S5). They are interpreted to be secondary in origin. Despite the absence of crosscutting relationships between Types 1 and 2 fluid inclusions, we interpret the Type 2 inclusions to postdate Type 1 inclusions because they occur along healed fractures crosscutting quartz grains boundaries.

Table 1 Summary of Types 1, 2, and 3 fluid inclusion characteristics

Aqueous-carbonic (H ₂ O-CO ₂)	Subtype 1a	Subtype 1b	Subtype 1c
System	CO ₂ -H ₂ O-NaClCO ₂ -H ₂ O-NaCl	CO ₂ -H ₂ O-NaClCO ₂ -H ₂ O-NaCl	CO ₂ -H ₂ O-NaClCO ₂ -H ₂ O-NaCl
Abundance	Rare	Rare	Rare
Size (mm)	3.9 to 14.0	5.0 to 10.6	4.0 to 17.3
V% CO ₂	10 to 25	40 to 50	70 to 95
TmCO ₂ (°C)	-57.1 to -56.7	-57.1 to -56.8	-57.4 to -56.6
Tmclath (°C)	5.2 to 6.5	5.8 to 6.7	5.0 to 6.5
Salinity (wt% NaCl eq.)	7.5 to 8.8	6.0 to 8.6	6.3 to 9.1
ThCO ₂ (°C)	17.8 to 31.1 (L)	22.1 to 31 (L)	8.7 to 29.4 (L)
Bulk density (g/cc)	0.93 to 0.95	0.83 to 0.89	0.64 to 0.87
Thtot (L) (°C)	240 to 261 (L) (<i>n</i> = 5)	253 to 330 (L) (<i>n</i> = 5)	–
Td (°C)	200 to 220 (<i>n</i> = 3)	263.3 (<i>n</i> = 2)	240 to 341 (<i>n</i> = 15)
Aqueous (H ₂ O-rich)	Type 2	Subtype 3a	Subtype 3b
System	H ₂ O-NaCl-CaCl ₂ H ₂ O-NaCl-CaCl ₂	H ₂ O-NaCl-CaCl ₂ H ₂ O-NaCl-CaCl ₂	Undetermined
Abundance	Common	Abundant	Abundant
Size (mm)	4.7 to 25.7	4.5 to 22.3	5.4 to 14.4
V% vapor phase	15 to 30	5	5
Te (°C)	<-50.0 to <-31.1	<-50 to <-40	
Tmice (°C)	-33.8 to -13.6		No freezing down to -180
Salinity (wt% NaCl eq.)	16.7 to 28.3	28.3 to 32.4	
Bulk density (g/cc)	1.15 to 1.23	1.23 to 1.50	
Th (L) (°C)		59.7 to 131.5 (<i>n</i> = 18)	
Tmdm (°C)		130.0 to 211.2 (<i>n</i> = 18)	
Thtot (L) (°C)	353.4 to 458.0 (<i>n</i> = 20)		50.2 to 127.5 (<i>n</i> = 8)
Td (°C)	353.1 to 523.0 (<i>n</i> = 13)		

V% percentage of the volume occupied, *Tm*CO₂ melting temperature of the carbonic phase, *Tm*clath melting temperature of the clathrate, *Th*CO₂ homogenization temperature of the carbonic phase to the liquid, *Thtot* total homogenization to the liquid (L) or the vapor (V) phase, *Td* decrepitation temperature, *Te* temperature of the eutectic, *Tm*ice melting temperature of ice, *Tmdm* dissolution temperature of the daughter mineral

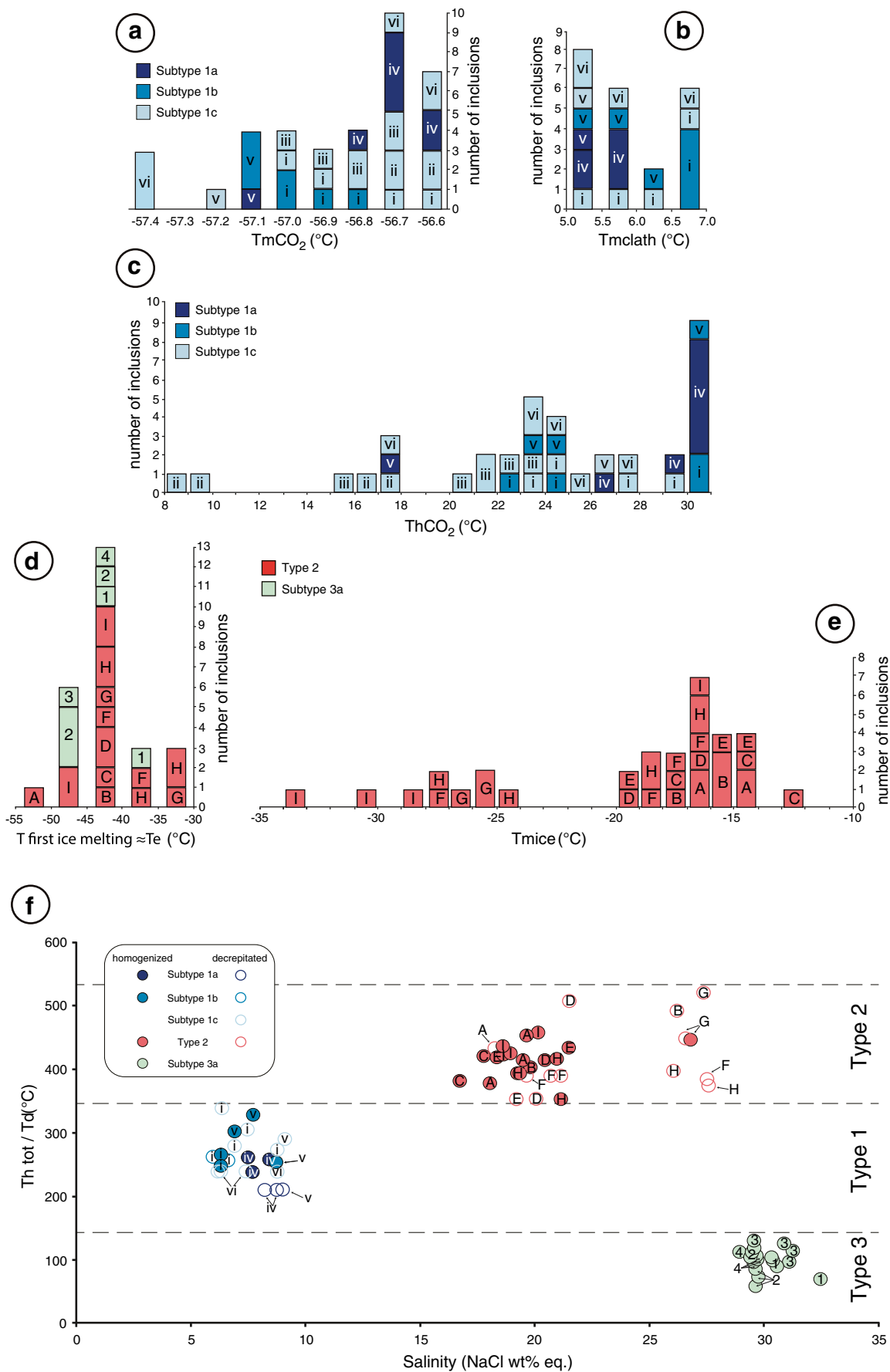
Type 3 aqueous fluids include two subtypes ranging from 5 to 25 μm in size with a square to elongated irregular shape (Figs. 8d, e, Tables 1 and S5). Subtype 3a consists of three phases at room temperature, including a liquid, a vapor, and a daughter mineral. Subtype 3b is composed of a liquid and a vapor phase at room temperature. The vapor typically fills 5 vol% of the inclusion. Type 3 FIAs contain coexisting subtypes 3a and 3b, and are located within healed fractures crosscutting quartz grain boundaries (Figs. 8d, e, Tables 1 and ESM 1: Table S5). There is a positive correlation between fracture density and Type 3 fluid inclusion abundance. Type 3 fluids are considered to be secondary in origin based on crosscutting quartz grain boundaries.

Fluid inclusion microthermometry

Type 1: aqueous-carbonic fluid inclusions

Melting of solid CO₂ (*Tm*CO₂) in subtype 1a inclusions occurs from -57.1 to -56.6 °C, from -57.1 to -56.8 °C for subtype 1b, and from -57.4 to -56.6 °C for subtype 1c (Fig. 9a,

Tables 1 and ESM 1: Table S5). The *Tm*CO₂ indicates small amounts of dissolved gas species in the carbonic phase. However, Raman spectroscopy of Type 1 inclusions did not reveal the presence of other dissolved gases, such as N₂ or CH₄; therefore, we conclude that the gas phase has a nearly pure CO₂ composition. Clathrate melting temperatures (*Tm*CLATH) range from +5.0 to +6.5 °C (Fig. 9b, Tables 1 and S5), yielding salinities from 6.0 to 9.1 wt% NaCl eq. using the equation of Diamond (1992) (Fig. 9f, Tables 1 and ESM 1: Table S5). The homogenization temperatures of CO₂ to liquid (*Th*CO₂ (L)) range between +26.6 and +31.0 °C in subtype 1a, +22.1 and +31.0 °C in subtype 1b, and +8.7 and +29.4 °C in subtype 1c inclusions (Fig. 9c, Tables 1 and S5), corresponding to density ranges of 0.93 to 0.95, 0.83 to 0.89, and 0.64 to 0.87, respectively (Tables 1 and S5), using the appropriate equations of state for the aqueous-carbonic system (Bowers and Helgeson 1983; Duan et al. 1992a; Bakker 1999) in Bakker's (2003) program. The liquid phase homogenized into liquid (*Th*TOT) between 240 and 261 °C for subtype 1a, and some inclusions decrepitated between 200 and 220 °C



◀ **Fig. 9** Microthermometric data for fluid inclusions in gold-bearing quartz veins at Lac Herbin. **a** T_{mCO_2} . **b** T_{mCLATH} . **c** T_{hCO_2} (L). **d** Temperature of observation of the first ice melting ($\approx T_e$). **e** T_{mICE} . **f** Final homogenization to the liquid phase (T_{hTOT}) and decrepitation temperatures (T_d) versus salinity. Numbers in the symbol correspond to the FIA numbers allocated for each FIA in the ESM 1: Table S5

(Fig. 9f, Tables 1 and ESM 1: Table S5). Subtype 1b inclusions homogenized to the liquid phase from 253 to 330 °C, and two inclusions decrepitated at 263.3 °C. All subtype 1c inclusions decrepitated between 240 and 341 °C.

To summarize, Type 1 aqueous-carbonic inclusions are modeled in the CO_2 - H_2O -NaCl system. Salinities are similar for each subtype, and their respective densities are in agreement with the filling proportion of the CO_2 phase with respect to the total fluid inclusion volume. However, the homogenization and decrepitation temperatures are scattered for subtypes 1b and 1c inclusions, respectively.

Type 2: high-temperature aqueous fluid inclusions

First ice melting, approximating the eutectic temperature (T_e), was observed between -50 and -31.1 °C (Fig. 9d, Tables 1 and ESM 1: Table S5), indicating that the fluid of Type 2 inclusions can be interpreted within the H_2O -NaCl- $CaCl_2$, H_2O -NaCl- $MgCl_2$ or H_2O -NaCl- $FeCl_2$ systems (Zhang and Frantz 1987). We prefer to attribute this fluid to the H_2O -NaCl- $CaCl_2$ system, because most first ice melting temperatures fall between -45 and -40 °C. Although we have not observed any metastable phases, we attribute the T_e value below -50 °C to the formation of metastable phases on freezing, as metastable melting events are typically reported at temperatures below -50 °C by Vanko et al. (1988), Davis et al. (1990), and Oakes et al. (1990).

The T_{mICE} range from -33.8 to -13.6 °C yielding salinities ranging from 16.7 to 28.3 wt% NaCl eq. (Figs. 9e, f, Tables 1 and ESM 1: Table S5) using the equation of Steele-MacInnis et al. (2011). These results are in agreement with results obtained with the equation of Oakes et al. (1990) using Bakker's (2003) program. As it was not possible to observe melting of hydrohalite, we calculated the salinities using a ratio $wt\%NaCl/(wt\%NaCl + wt\%CaCl_2)$ of 0.99 because of the similar effect of NaCl or $CaCl_2$ on ice melting (Shepherd et al. 1985). Salinities using a ratio $wt\%NaCl/(wt\%NaCl + wt\%CaCl_2)$ of 0.5 were also calculated and show no significant differences (ESM 1: Table S5). Density is between 1.15 and 1.23 g/cm^3 using the appropriate equations of state for the system H_2O -NaCl- $CaCl_2$ (Zhang and Frantz 1987). The T_{hTOT} to the liquid are between 353 and 458 °C, most of them between 410 and 430 °C. Some inclusions decrepitated (T_d) between 353 and 523 °C. Raman spectroscopy indicates that the vapor phase is composed of pure H_2O , which is consistent with the absence of clathrate formation during cooling of Type 2 inclusions.

Type 3: low-temperature aqueous fluid inclusions

Subtype 3a inclusions yield a first ice melting temperature (T_e) between -50 and -40 °C, whereas T_{hTOT} to the liquid phase are between 59.7 and 131.5 °C, lower than the dissolution temperature of daughter minerals ranging from 110.0 to 211.2 °C (Fig. 9f, Tables 1 and ESM 1: Table S5). Only the dissolution temperature of daughter mineral was measured for these inclusions. Salinities range between 28.3 and 32.4 wt% NaCl eq. using the H_2O -NaCl system, with a density ranging between 1.23 and 1.50 g/cm^3 (Table 1 and ESM 1: Table S5). Salinities and densities were calculated using the appropriate equations of state for H_2O -NaCl (Knight and Bodnar 1989; Archer 1992; Bodnar 1993; Bodnar and Vityk 1994) using Bakker's (2003) program. Within the same FIA, subtype 3b inclusions have homogenization temperatures to the liquid between 50.2 and 127.5 °C. These inclusions have a metastable behavior, they did not freeze down to -180.0 °C, and the vapor phase did not nucleate back after total homogenization (Tables 1 and ESM 1: Table S5).

Discussion

Timing of the mineralized veins

Belkabit et al. (1993) suggested that dikes were a major rheologic control on the emplacement of the shear zone-hosted auriferous veins cutting the Bourlamaque batholith at the Dumont-Bras d'Or, New Formaque, and Ferderber deposits (Fig. 2). However, at the Lac Herbin deposit, Lemarchand et al. (2010) showed that the main mineralized structures associated with felsic and/or mafic dikes were emplaced along a preexisting fault. By contrast, Lemarchand et al. (2010) concluded that the emplacement of subsidiary mineralized structures is controlled by a preferential direction along dikes. According to Lemarchand (2012), the overall vein geometry and kinematic indicators suggest a cogenetic formation of all mineralized structures throughout the deposit. The associated extensional veins and tourmaline fibers direction are compatible with formation under a N-S- to SW-NE-oriented subhorizontal main stress (σ_1), consistent with formation during the late stage of the D2 regional deformation (Robert 1994). The maximum age for the emplacement of the gold-bearing veins is constrained by the $^{40}Ar/^{39}Ar$ amphibole cooling age of the mafic dikes at ca. 2666–2670 Ma (Lemarchand 2012), which constrain the gold mineralization to be younger than the regional metamorphism bracketed by U-Pb zircon ages between 2697 ± 19 and 2682 ± 8 Ma (Claoué-Long et al. 1990). The age of the “late” ore-forming fracture filling event remains unconstrained and discussed below.

Significance and relative temporal relationship of fluid inclusion types

Type 1 aqueous-carbonic inclusions have variable CO₂ total volume ratios even within a single FIA (Fig. 8a; Tables 1 and ESM 1: Table S5). Two mechanisms are considered to explain this observation: (1) fluid immiscibility and (2) post-entrapment modifications. The vein system at the Lac Herbin deposit was likely emplaced under fluctuating fluid pressure conditions as suggested by Sibson et al. (1988) for the Val-d'Or district, which is certainly a favorable environment for fluid immiscibility. However, the three subtypes recognized for Type 1 inclusions and coexisting in the same FIA have highly variable final homogenization and decrepitation temperatures, but a narrow range of salinities (Figs. 8a and 9f, Tables 1 and ESM 1: Table S5), which is at variance with the immiscibility criterion suggested by Ramboz et al. (1982). Therefore, our results support post-entrapment modifications of the fluid inclusions, which are consistent with the intense deformation that affected the shear zones and also with previous experimental studies by Pêcher and Boullier (1984) and Bakker and Jansen (1991), who interpreted scattered Th_{TOT} and Th_{CO₂} in terms of reequilibration of aqueous-carbonic inclusions. Bakker and Jansen (1991) suggested post-entrapment modifications of aqueous-carbonic inclusions by preferential water leakage resulting in enrichment in CO₂ with respect to the original composition of the inclusions, which can explain scattered L/V ratios in heterogeneous Type 1 FIAs. Indeed, despite the lack of textural evidence for post-entrapment modifications, our microthermometric results reveal an increase in Th_{TOT} coupled with scattered Th_{CO₂} from subtype 1a to subtype 1c inclusions (Figs. 9c, f, Tables 1 and ESM 1: Table S5). The Th_{CO₂} and Th_{TOT} from homogeneous FIAs of subtype 1a inclusions are relatively constant, whereas heterogeneous FIAs show significant variation of Th_{TOT}, up to 100 °C among the same FIA. Therefore, based on the lack of evidence for fluid immiscibility and considering the compressional strain affecting the mineralized shear zones and the microthermometry results, the post-entrapment modifications scenario of Type 1 inclusions is preferred at the Lac Herbin deposit; however, we cannot definitely rule out fluid immiscibility (Pêcher and Boullier 1984; Bakker and Jansen 1991; Bodnar 2003; Tarantola et al. 2010; Diamond et al. 2010).

High-temperature Type 2 aqueous fluid inclusions are interpreted to postdate Type 1 inclusions based on their occurrences within fractures crosscutting quartz grain boundaries, in contrast to Type 1 fluid inclusions which only occur as intragrain clusters, and their distinctly higher homogenization temperatures (Figs. 8b, c, 9d–f, Tables 1 and ESM 1: Table S5). In earlier studies on other locations within the Val-d'Or mining district, Robert and Kelly (1987), Robert et al. (1995), and Boullier et al. (1998) interpreted similar high-temperature aqueous fluid as the residual end-member fluid after phase

separation of an aqueous-carbonic fluid, with a similar composition to the one of subtype 1a at Lac Herbin. In the case of the Lac Herbin deposit, the intermediate to high salinity Type 2 fluid inclusions (16.7 to 28.3 wt% NaCl eq.) and their high homogenization (380 to 458 °C) and decrepitation (353.1 to 523 °C) temperatures are unlikely to be related to Type 1 inclusions by phase separation, because of distinctly lower Th_{TOT} and decrepitation temperatures ranging between 200 and 341 °C (Fig. 9, Tables 1 and ESM 1: Table S5). The Type 2 inclusions have scattered Th_{TOT} within the same FIA (Fig. 9, Tables 1 and ESM 1: Table S5), which suggest that post-entrapment modifications of the inclusions have occurred. We interpret the Type 2 inclusion as a distinct hydrothermal fluid, temporarily unrelated to the Type 1 hydrothermal fluid. The significantly higher temperature of the hydrothermal event recorded by Type 2 inclusions can be a cause for the post-entrapment modification of the Type 1 fluid inclusions.

The low-temperature Type 3 aqueous inclusions are considered as secondary, postdating Types 1 and 2 inclusions because of their low homogenization temperatures, their high salinity, their systematic occurrence within fractures and they form distinct assemblages (Figs. 8d, e, 9f, Tables 1 and ESM 1: Table S5). The melting temperature of daughter minerals in subtype 3a inclusions is interpreted as a reliable minimum trapping temperature, ranging from 135 to 211 °C (Tables 1 and ESM 1: Table S5). This low-temperature aqueous fluid is similar to the Ca-Na-Cl-rich groundwaters described in the Canadian Shield and sampled at several gold mines (Frape et al. 1984; Frape and Fritz 1987; Kerrich and Kamineni 1988; Kyser and Kerrich 1990; Boullier et al. 1998). Therefore, this fluid is considered to be trapped late in the hydrothermal history of the Lac Herbin deposit, postdating gold introduction and precipitation.

Fluid evolution of the hydrothermal system at the Lac Herbin deposit

Isochores were calculated for each inclusion type according to Bakker (2003). They allow us to constrain the sequence of fluid events in terms of pressure and temperature at the Lac Herbin deposit (Fig. 10). As discussed above, the Type 1 aqueous-carbonic fluid inclusions are interpreted to be the earliest, followed by the Type 2 high-temperature aqueous fluid inclusions, and finally by the Type 3 low-temperature aqueous fluid inclusions. Considering the postentrapment modifications concluded for subtype 1a inclusions, the homogenization temperatures of 250–300 °C represent the minimum temperature estimate of entrapment (Fig. 10). Assuming a depth of formation of 8 to 10 km for orogenic gold deposits (e.g., Groves et al. 1998, 2003; McCuaig and Kerrich 1998; Goldfarb et al. 2005; Robert et al. 2005), the minimum pressure of entrapment must have been between 80 and 100 MPa under a hydrostatic regime, or between

210 and 260 MPa under a lithostatic regime. Isochores for high-temperature Type 2 fluids plot separately in P-T space with respect to Type 1 inclusions (Fig. 10). Therefore, Type 2 fluid inclusions most likely represent a different hydrothermal fluid emplaced at higher temperature than the hydrothermal fluid at the origin of Type 1 inclusions. The pressure corrections have not been performed; therefore, the Th_{TOT} is interpreted as minimum trapping temperatures of 350 °C. The low-temperature Type 3 aqueous fluids are interpreted to be late in the vein system evolution, with an average minimum entrapment temperature at ~100 °C (Fig. 10).

Comparison with previous studies in the Val-d’Or district

Previous fluid inclusion studies in the Val-d’Or district were carried out on gold-bearing veins at the Donalda (Chi et al. 1992), Sigma (Robert and Kelly 1987; Firdaous 1995; Olivo et al. 2006), Dumont-Bras d’Or (Firdaous 1995), Siscoe (Olivo and Williams-Jones 2002), Orenada #2 (Neumayr and Hagemann 2002; Neumayr et al. 2007), and Cartier-Malartic and Paramaque deposits (Neumayr et al. 2007). Boullier et al. (1998) and Olivo et al. (2006) described fluids in barren veins, respectively, at the Donalda and Sigma deposits. A summary of microthermometry data of studies carried out at the Sigma, Siscoe, Dumont-Bras d’Or, and Donalda deposits is given in Table 2. The three types of fluid inclusions found in the mineralized veins of the Lac Herbin deposit have similar physical and chemical properties than those described in the other deposits of the Val-d’Or mining district (Tables 1 and 2).

Robert and Kelly (1987), Robert et al. (1995), Firdaous (1995), Boullier et al. (1998), Neumayr and Hagemann (2002), and Neumayr et al. (2007) suggested fluid immiscibility to explain the coexistence of vapor-rich aqueous-carbonic inclusions (such as subtype 1c inclusions at Lac Herbin) and liquid-rich aqueous inclusions (such as Type 2 at Lac Herbin). The “high”-temperature aqueous fluid at the Sigma deposit was interpreted as the aqueous end-member of the unmixed aqueous-carbonic parent fluid (Robert et al. 1995; Boullier et al. 1998). At the Donalda deposit, however, Boullier et al. (1998) attributed the high-temperature aqueous inclusions to hot fluid infiltration within the barren Proterozoic vein. Furthermore, no high-temperature aqueous fluid was reported for the mineralized veins at the Dumont-Bras d’Or deposit (Firdaous 1995) and at the Orenada #2 deposit (Neumayr and Hagemann 2002). The distinction of low- and high-temperature data sets is variable in the different contributions (Robert and Kelly 1987; Robert et al. 1995; Firdaous 1995; Boullier et al. 1998; Olivo et al. 2006). For the sake of comparison, we attempted to systematically compare data ranges of previous studies in Table 2.

The heterogeneous Type 1 FIAs including three subtypes illustrate post-entrapment modifications of subtype 1a to subtype 1c based on the following reasons: (1) variable CO₂ volume contents, (2) scattered Tm_{CO_2} and Th_{TOT} , and (3) similar salinities. Our study shows that the aqueous-carbonic subtype 1a fluid inclusions represent the earliest hydrothermal fluid, and therefore responsible for the post-peak regional metamorphism main vein filling auriferous event at or after 2682 ± 8 Ma (Claoué-Long et al. 1990). This is in agreement with the previous studies carried out in the Val-d’Or district (Robert and Kelly 1987; Robert et al. 1995; Firdaous. 1995;

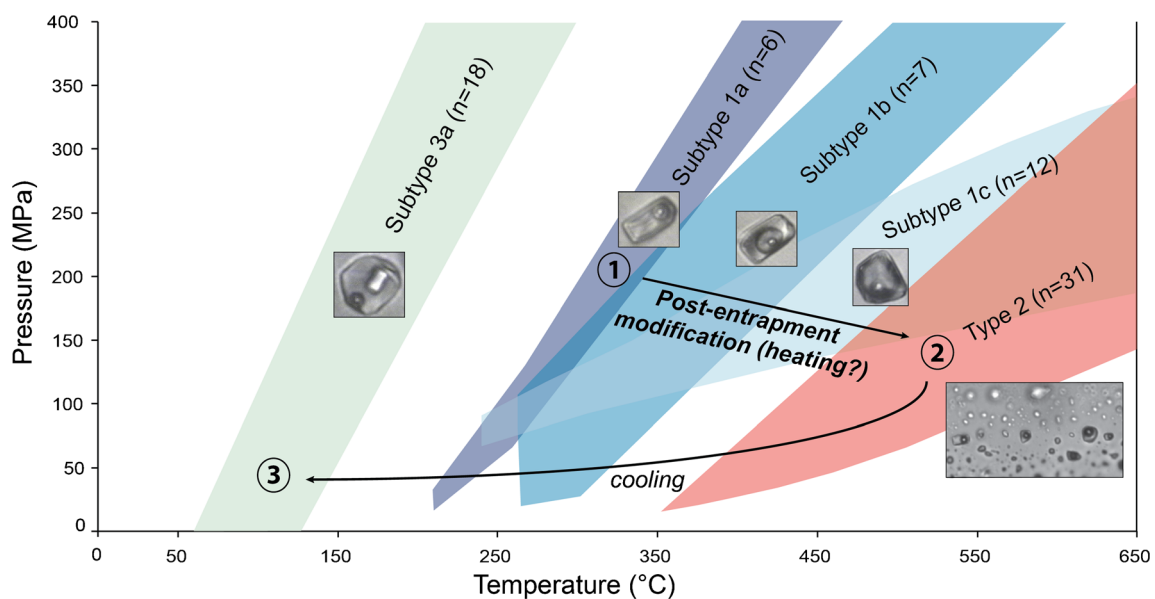


Fig. 10 Isochore interpretation for postentrapment modifications of Type 1 inclusions followed by entrapment of Types 2 and 3 inclusions

Table 2 Compilation of fluid inclusion characteristics from previous studies at Sigma (Robert and Kelly 1987; Firdaus 1995; Robert et al. 1995; Olivo et al. 2006), Donald (Chi et al. 1992; Boullier et al. 1998), Dumont-Bras-d'Or (Firdaus 1995), and Siscoe mines (Olivo and Williams-Jones 2002)

	Robert and Kelly (1987)—Sigma auriferous veins	Firdaus. (1995)—Sigma Auriferous veins	Robert et al. (1995)—Sigma Fault vein	Robert et al. (1995)—Sigma Extensional vein	Olivo (2006)—Sigma Barren veins	Olivo (2006)—Sigma Auriferous veins
System	CO ₂ -H ₂ O-NaCl±CH ₄ CO ₂ -H ₂ O-NaCl±CH ₄	CO ₂ -H ₂ O-NaCl±CH ₄ CO ₂ -H ₂ O-NaCl±CH ₄	CO ₂ -H ₂ O-NaCl±CH ₄ CO ₂ -H ₂ O-NaCl±CH ₄	CO ₂ -H ₂ O-NaCl±CH ₄ CO ₂ -H ₂ O-NaCl±CH ₄	CO ₂ -H ₂ O-NaClCO ₂ -H ₂ O-NaCl	CO ₂ -H ₂ O-NaCl±CH ₄ CO ₂ -H ₂ O-NaCl±CH ₄
Occurrence	Healed fractures and 3D clusters	–	3D clusters	3D clusters	Rare and secondary	Abundant and secondary
V% CO ₂	20 to 80 (mean 40–60)	–	20 to 85	10 to 85	5 to 45	5 to 45
TmCO ₂ (°C)	–58 to –56.6 °C (mean –57.5 to –57 °C)	–63.7 to 56.7 °C	–58.3 to –56.8 °C	–63.7 to –56.7 °C	–56.8 °C	–58.3 to –56.2 °C
Tmclath/salinity	4.5 to 10 °C/2 to 9 wt% NaCl eq.	6.4 to 14.7 °C	7.2 to 8.8 °C/1 to 4 wt% NaCl eq.	6.4 to 14.7 °C/2 to 6 wt% NaCl	1.3 wt% NaCl eq.	6 to 10 °C/4 to 5 wt% NaCl eq.
ThCO ₂ /density	–8 to 31 °C (mean >14 °C)	–49.2 to 30.9 °C	11.5 to 29.9 °C/0.67 to 0.99	–49.2 to 30.9 °C/0.47 to 1	–	–9.8 to 30 °C (mean 20–30 °C)
Thtot (L or V)	185 to 395 °C (L or V)	211.5 to 425 °C (L or V)	237 to 320 °C (L or V)	211 to 425 °C (L or V)	>350 °C (L)	228 to 440 °C (mean 228 to 270 °C) (L)
Td	–	202 to 398.2 °C	260 to 340 °C	202 to 335 °C	345 °C	345 °C
System Occurrence	CO ₂ -CH ₄ CO ₂ -CH ₄ Healed fractures and 3D clusters	CO ₂ -CH ₄ CO ₂ -CH ₄ Healed fractures and 3D clusters	CO ₂ -CH ₄ CO ₂ -CH ₄ Healed fractures and 3D clusters	CO ₂ -CH ₄ CO ₂ -CH ₄ Healed fractures and 3D clusters	CO ₂ -CH ₄ CO ₂ -CH ₄ Rare and secondary	CO ₂ -CH ₄ CO ₂ -CH ₄ Abundant and secondary
TmCO ₂	–62 to –56.6 °C (mean –57.5 to –57 °C)	–63 to –56.7 °C	–58.1 to –57 °C	–63 to –56.7 °C	–56.6 °C	–57.5 to –56.3 °C
Tmclath/salinity	–	–	–	–	8.9 °C/2.6 wt% NaCl eq.	4.6 to 9 °C/2.1 to 10 wt% NaCl eq.
ThCO ₂ /density	–33.1 to 31 (mean 2)/0.65 to 1.07	–49.2 to 29.6 °C	–27.5 to 28.2 °C (L or V)/0.52 to 1	–49.2 to 28.8 °C (L)/0.6 to 1.03	–	–11.3 to 30 °C
System	H ₂ O-NaCl-CaCl ₂ -H ₂ O-NaCl-CaCl ₂	H ₂ O-NaCl-CaCl ₂ H ₂ O-NaCl-CaCl ₂	H ₂ O-NaCl-CaCl ₂ H ₂ O-NaCl-CaCl ₂	H ₂ O-NaCl-CaCl ₂ H ₂ O-NaCl-CaCl ₂	H ₂ O-NaCl-CaCl ₂ H ₂ O-NaCl-CaCl ₂	H ₂ O-NaCl-CaCl ₂ H ₂ O-NaCl-CaCl ₂
Type Occurrence	Healed fractures	High T°	Healed fractures	Healed fractures	High and low T°	High and low T°
V% vapor phase	5	–	–	–	–	–
Te	–68 to –55 °C	–72 to –45.9 °C	–78 to –32.8 °C	–61.8 to –43.7 °C	–49.2 to –30 °C	–30 to –69.4 °C
Tmice	–	–51.2 to –1 °C	–49.4 to –1 °C	–46.4 to –3.2 °C	–33.9 to 0 °C	–55 to –0.4 °C
Salinity	25 to 34 wt% NaCl eq.	5 to 30 wt% NaCl eq.	2 to 40 wt% NaCl eq.	5 to 31 wt% NaCl eq.	0 to 23 wt% NaCl eq.	0 to 23 wt% NaCl eq.
Thtot (L)	60 to 295 °C	249.2 to 366.9 °C	60.5 to 222 °C	177 to 204 °C	137 to 303 °C	175–225 °C/300–375 °C/16.4–327 °C
Td	140 to 235 °C	–	179 to 220 °C	179 to 220 °C	345 °C	207 to 400 °C
Tmtdm Bulk density (g/cc)	–	–	<160 °C (L) 0.94 to 1.26	<180 °C and >180 °C (L) 0.58 to 1.2	–	–
Interpretation	Unmixing by pressure drop of homogeneous auriferous H ₂ O-CO ₂ parent fluid resulting in entrapment of contemporaneous CO ₂ -rich and H ₂ O-NaCl-CaCl ₂ fluid inclusions	Unmixing by pressure drop of homogeneous auriferous H ₂ O-CO ₂ parent fluid resulting in entrapment of contemporaneous CO ₂ -rich and H ₂ O-NaCl-CaCl ₂ fluid inclusions	Unmixing by pressure drop of homogeneous auriferous H ₂ O-CO ₂ parent fluid resulting in entrapment of contemporaneous CO ₂ -rich and H ₂ O-NaCl-CaCl ₂ fluid inclusions	Unmixing by pressure drop of homogeneous auriferous H ₂ O-CO ₂ parent fluid resulting in entrapment of contemporaneous CO ₂ -rich and H ₂ O-NaCl-CaCl ₂ fluid inclusions	–	Auriferous CO ₂ -rich fluid diluted by high temperature H ₂ O-rich fluids

Table 2 (continued)

	Chi et al (1992)—Donalda Auriferous veins	Boullier et al. (1998)—Donalda Proterozoic barren quartz vein	Firdaus. (1995)—Dumont/ Bras d'or Auriferous veins	Olivo & Williams-Jones (2002)—Siscoe Auriferous veins
System	CO ₂ -H ₂ O-NaCl ± CH ₄	—	CO ₂ -H ₂ O-NaCl ± CH ₄	CO ₂ -H ₂ O-NaCl ± CH ₄
Occurrence	—	—	—	Healed fractures
V% CO ₂	—	—	—	15 to 85 (mean 15–30)
TmCO ₂ (°C)	–57.7 to –56.9 °C	—	–58.2 to –56.6 °C	–58.5 to –56.5 °C
Tmclath/salinity	3.4 to 8.9 °C	—	–3.8 to 4.5 °C	5.5 to 9.9 °C/4 to 10 wt% NaCl eq.
ThCO ₂ /density	–23.3 to 30.5 °C	—	–0.4 to 30 °C	6.5 to 31 °C/0.5 to 0.9
Thot (L or V)	125 to 367 °C (L)	—	211.4 to 376.8 °C (L)	156 to 330 °C (L)
Td	—	—	238 to 397.6 °C (L)	180 to 369 °C
System	CO ₂ -CH ₄	—	CO ₂ -CH ₄	CO ₂ -CH ₄
Occurrence	–57.5 to –57.2 °C	—	—	Healed fractures
TmCO ₂	8.3 °C/Low salinity	—	–56.8 °C	–56.6 °C
Tmclath/salinity	–30.2 to 28.4 °C	—	–8.8 to 5 °C	–8 to 8.8 °C
ThCO ₂ /density	204 to 328 °C	—	H ₂ O-NaCl-CaCl ₂	H ₂ O-NaCl
System	H ₂ O-NaCl-CaCl ₂	H ₂ O-NaCl-CaCl ₂	Low T _o	—
Type	High and low temperatures	High T _o	Healed fractures	Healed fractures
Occurrence	—	3D clusters - healed fractures	5 to 10	5 to 30
V% vapor phase	—	—	–77 to –28.8 °C	–22 °C
Te	<–50 °C	–67.4 to –47 °C	–52.8 to –2.4 °C	–4 to –1 °C
Tmice	–40.3 to –2.4 °C	–32.6 to –6 °C	2 to 40 wt% NaCl eq.	2 to 6 wt% NaCl eq.
Salinity	—	15 to 28 wt% NaCl eq.	15 to 35 wt% NaCl eq.	95 to 249 °C
Thot (L)	100 to 380 °C (mean 160 to 220 °C)	212 to >450 °C	29.6 to 186.8 °C	—
Td	—	—	—	—
Tmdm	—	—	115 to 186.8 °C	—
Bulk density (g/cc)	—	—	—	—
Interpretation	Unmixing of homogeneous auriferous H ₂ O-CO ₂ parent fluid resulting in entrapment of CO ₂ -rich and H ₂ O-NaCl-CaCl ₂ fluid inclusions (interpretation by Boullier et al. 1998)	—	Auriferous H ₂ O-CO ₂ and CO ₂ -rich fluids but no phase immiscibility involved.	Mixing of an auriferous CO ₂ -H ₂ O-NaCl fluid with a contemporaneous barren CO ₂ -H ₂ O-NaCl-CH ₄ fluid recycled from the wall-rock.

V% percentage of the volume occupied, TmCO₂ melting temperature of the carbonic phase, Tmclath melting temperature of the clathrate, ThCO₂ homogenization temperature of the carbonic phase to the liquid, Thot total homogenization to the liquid (L) or the vapor (V) phase, Td decrepitation temperature, Te temperature of the eutectic, Tmice melting temperature of ice, Tmdm dissolution temperature of the daughter mineral

Boullier et al. 1998; Neumayr and Hagemann 2002; Neumayr et al. 2007; Olivo et al. 2006). We do not have evidence for fluid immiscibility or fluid mixing as a mineral deposition mechanism; instead, we propose a cooling and/or fluid-rock interaction deposition processes. The presence of heterogeneous Type 1 FIAs including subtypes 1a, 1b, and 1c is ascribed to post-entrapment modification processes. The high-temperature fluid inclusions do not represent the aqueous phase of an immiscibility process as it has been suggested by previous studies (Robert and Kelly 1987; Robert et al. 1995; Firdaous. 1995). The Type 2 fluid inclusions display higher Th_{TOT} , and the isochores suggest P-T conditions different from those of the CO_2 -bearing Type 1 fluid inclusions (Fig. 10). Mixing of the CO_2 -bearing and the high-temperature aqueous fluids was suggested for the Sigma deposit (Olivo et al. 2006), but it is not observed in this study. At the Lac Herbin deposit, the distinct separate distribution of Types 1 and 2 data points corresponding to unrelated FIAs, with a major gap between both data sets in the Th_{TOT} vs. salinity diagram (Fig. 9f), is interpreted as a strong argument against fluid mixing. Boullier et al. (1998) and Olivo et al. (2006) at the Donalda and Sigma deposits, respectively, reported aqueous high-temperature with rare to no CO_2 -bearing inclusions in barren veins, and Olivo et al. (2006) have shown that the high-temperature aqueous fluid at the Sigma deposit were metal-poor based on laser ablation inductively coupled plasma mass spectrometry (LA-ICP-MS) analyses. In addition, Mulja (1995) reported a similar late barren, high-temperature calcic fluid in the Mo-, Li-, U-, and Be-bearing pegmatites from four peraluminous monzogranite intrusions in the Preissac-Lacorne batholith. These fluids were attributed to contact metamorphism associated with the emplacement of the Preissac-Lacorne batholith (S-type granite) at ca. 2645–2611 Ma. Consequently, we conclude that the high-temperature aqueous Type 2 fluid described in the Lac Herbin deposit displays similarities that are comparable to the barren calcic fluid described by Mulja (1995), Boullier et al. (1998), and Olivo et al. (2006). Therefore, we interpret the high-temperature aqueous fluid inclusions as a distinct hydrothermal fluid unrelated and postdating the Type 1 fluid inclusions.

Remobilization of gold during late, high-temperature, aqueous saline fluid infiltration at Lac Herbin?

Six hornblendes from the Bourlamaque batholith-hosted Lac Herbin deposit yield two age groups, respectively, at 2692–2681 and 2650–2613 Ma (Lemarchand 2012). The older age group is close to the minimum U-Pb zircon age at 2699 Ma of the synvolcanic intrusion (Wong et al. 1991) and was likely disturbed by regional greenschist metamorphism (Lemarchand 2012). The younger amphiboles represent a subsequent thermal event, which overlaps with the age of contact

metamorphism associated with S-type granites, such as the Preissac-Lacorne batholith at ca. 2645–2611 Ma (Feng et al. 1992; Kerrich and King 1993; Chown et al. 2002). At the Lac Herbin deposit, $^{40}Ar/^{39}Ar$ geochronology on muscovite yields ages between 2615 and 2500 Ma, with two main peaks at 2585–2565 and 2523–2512 Ma (Lemarchand 2012). Similar muscovite and biotite $^{40}Ar/^{39}Ar$ ages, and rutile U-Pb ages were obtained at the Camflo (Zweng et al. 1993) and Sigma deposits (Hanes et al. 1992). The difference in age between amphibole from the Bourlamaque batholith and hydrothermal muscovite is likely a consequence of high-temperature fluid migration, recorded by the Type 2 fluid described at the Lac Herbin deposit (Th_{TOT} of 350 to 460 °C). Such a high-temperature fluid event may have affected the muscovite geochronometer, which has a closure temperature between 410 and 490 °C (Harrison et al. 1985), but not that of amphibole, which has a higher closure temperature between 500 and 550 °C (Harrison and Fitzgerald 1986; Chiaradia et al. 2013). The younger muscovite ages likely correspond to a fluid circulation event during late-peak to post-peak contact metamorphism associated with the emplacement of S-type granites in the Val-d'Or mining district.

Two main mineralizing stages are documented at the Lac Herbin deposit. The main vein filling is attributed to syn- to post-peak regional metamorphism, whereas the late fracture filling corresponds to a late fluid introduction coeval with or post-dating local, younger contact metamorphism. The late fracture-filling paragenesis must be related to Ca-rich brines, because precipitation of carbonates is coeval with gold and chalcopyrite ± tellurides, pyrrhotite, sphalerite, pyrite, galena, and cobaltite. Based on our fluid inclusion data and observations, the high-temperature Type 2 fluid belongs to the H_2O -NaCl-CaCl₂ system and is trapped in secondary inclusions crosscutting quartz boundaries. Therefore, we conclude that the high-temperature aqueous Type 2 fluid likely represents a Ca-rich fluid, which is interpreted to act as a remobilizing agent for previously precipitated gold, and that may have perturbed the muscovite geochronometer at Lac Herbin. However, further research needs to be conducted to quantify these processes.

Two scenarios may explain the late fracture filling mineralizing event. The first scenario involves a separate and new pulse of auriferous hydrothermal fluid introducing and depositing large amounts of late gold in fractures associated with carbonates. By comparison with the first mineralizing event, a large amount of hydrothermal fluid would probably be required to introduce and precipitate the large quantity of gold precipitated during the fracture-filling event. The lack of hydrothermal alteration overprint, and the absence of an overgrowing, new quartz generation (as documented by the CL images) during the fracture-filling event, as well as the significant formation of late carbonate veins with gold, telluride, and base metals argues against the first scenario. Our second

and preferred scenario involves a local fluid migration event through the Val-d'Or mining district, recorded by the high-temperature Type 2 fluid, during or after contact metamorphism and linked to the S-type granite intrusions at 2645–2610 Ma. The high-temperature aqueous fluid, with intermediate to high salinities, certainly had the adequate chemistry to dissolve the previously precipitated gold of the main filling stage, and subsequently transport and reprecipitate it within pyrite and quartz fractures (Stefánsson and Seward 2004; Pokrovski et al. 2014). At temperature ranging from 400 to 500 °C, a pressure of 100 MPa and a moderate salinity, the most important ligand responsible for gold dissolution and transportation, is AuCl_2^- ; however, $\text{Au}(\text{HS})_2^-$, AuHS^0 , and AuOH^0 ligands are also considered (Stefánsson and Seward 2004; Williams-Jones et al. 2009; Pokrovski et al. 2014). Those conditions can be reconciled with the P-T conditions of the Type 2 fluid (Fig. 10); therefore, the high-temperature aqueous fluid, with intermediate to high salinities, is a good candidate to act as a remobilizing agent for gold that precipitated previously during the main vein filling gold-bearing stage.

Furthermore, the similar ore paragenesis and the similar chemical composition of gold and tellurides (ESM 1: Tables S3 and S4) suggest that gold, sulfide, and tellurides from the earlier, main vein filling stage, were dissolved, transported, and reprecipitated by the late, high-temperature hydrothermal fluid within late fractures at the deposit scale. We conclude that the remobilization process was intimately linked to the intrusion of the late S-type granites and was likely a local process restricted to the Val d'Or gold deposits. In order to test this interpretation, a comparison of orogenic gold deposits from different districts with and without neighboring late S-type granite intrusions could help to clarify such temporal fluid relationships and remobilization processes.

Conclusions

The Lac Herbin orogenic gold deposit is similar in terms of structural setting, vein textures, mineralogy, and fluids with respect to other deposits hosted in the Val-d'Or mining district, Abitibi greenstone belt. The paragenetic sequence includes a classic example of the main vein filling with abundant quartz, tourmaline, pyrite, and minor gold-tellurides, sulfides, and carbonates, followed by a fracture event, filled by chalcopyrite, gold, and Fe-Mn-carbonates associated with minor base metals or tellurides.

The fluid inclusion study at the Lac Herbin deposit allows us to offer an alternative model to fluid immiscibility and fluid mixing scenarios to explain ore forming processes in the Val-d'Or mining district. Three unrelated hydrothermal fluids were recognized in this study. An early aqueous-carbonic fluid (subtype 1a) is interpreted as the auriferous fluid present

during the early, main vein filling stage. Fluid inclusions that had trapped the early aqueous-carbonic fluid were partly reequilibrated during later temperature (and pressure) evolution of the Lac Herbin geological environment, as documented by subtypes 1b and 1c aqueous-carbonic inclusions. Together with the regional shear strain, the migration of a late, aqueous high-temperature Type 2 Ca-rich fluid with intermediate to high salinities is likely responsible for the post-entrapment modifications of the earlier Type 1 fluid inclusions and also acted as a remobilization agent for gold from the early vein stage into late fractures. The introduction of the high-temperature fluid in the Lac Herbin environment is attributed to syn- to post-contact metamorphism associated with the emplacement of S-type granites in the Val-d'Or mining district. Finally, a late, low-temperature saline aqueous fluid unrelated to precipitation and remobilization of gold, similar to those described elsewhere in the Canadian Shield, migrated through the granodioritic Bourlamaque batholith-hosted gold veins and is unrelated to gold deposition.

Acknowledgments This research was supported by a Discovery Grant to Georges Beaudoin from the Natural Science and Engineering Research Council of Canada, and the Bourse Lombard and the société académique des sciences naturelles of Switzerland delivered research grants to Hervé Rezeau. The authors are grateful to QMX Gold Corp. staff, Claude Gobeil and Jérémie Lemarchand, for kindly hosting and guiding at the mine. Kalin Kouzmanov (University of Geneva) conducted Electron Probe Microanalyses and Jean-Marie Boccard (University of Geneva) made the preparation of polished and doubly polished sections. Constructive comments by journal editor B. Lehmann and thoughtful reviews by Steffen Hagemann and Wei Jian significantly improved the content and the clarity of the manuscript.

References

- Anglin C, Jonasson I, Franklin J (1996) Sm-Nd dating of scheelite and tourmaline; implications for the genesis of Archean gold deposits, Val d'Or, Canada. *Econ Geol* 91:1372–1382
- Archer DG (1992) Thermodynamic properties of the $\text{NaCl} + \text{H}_2\text{O}$ system II. Thermodynamic properties of NaCl (aq), $\text{NaCl}\cdot 2\text{H}_2\text{O}$ (cr), and phase equilibria. *J Phys Chem* 21:793–829
- Ayer J, Amelin Y, Corfu F, Kamo S, Ketchum J, Kwok K, Trowell N (2002) Evolution of the southern Abitibi greenstone belt based on U–Pb geochronology: autochthonous volcanic construction followed by plutonism, regional deformation and sedimentation. *Precambrian Res* 115:63–95
- Bakker RJ (1999) Adaptation of the Bowers and Helgeson (1983) equation of state to the $\text{H}_2\text{O}\text{--CO}_2\text{--CH}_4\text{--N}_2\text{--NaCl}$ system. *Chem Geol* 154:225–236
- Bakker RJ, Package FLUIDS 1 (2003) Computer programs for analysis of fluid inclusion data and for modelling bulk fluid properties. *Chem Geol* 194:3–23
- Bakker RJ, Jansen JBH (1991) Experimental post-entrapment water loss from synthetic $\text{CO}_2\text{--H}_2\text{O}$ inclusions in natural quartz. *Geochim Cosmochim Acta* 55:2215–2230
- Beaudoin G, Rollion-Bard C, Giuliani G (2013) The boron isotope composition of tourmaline from the Val-d'Or orogenic gold deposits, Québec, Canada In: Jonsson E (ed) 12th Biennial SGA Meeting,

- Mineral Deposits Research for a High-Tech World. Uppsala, Sweden, pp. 1090–1092
- Beaudoin G, Pitre D (2005) Stable isotope geochemistry of the Archean Val-d'Or (Canada) orogenic gold vein field. *Miner Deposita* 40:59–75
- Belkabit A, Robert F, Vu L, Hubert C (1993) The influence of dikes on auriferous shear zone development within granitoid intrusions: the Bourlamaque pluton, Val-d'Or district, Abitibi greenstone belt. *Canadian J Earth Sci* 30:1924–1933
- Bodnar RJ (2003) Reequilibration of fluid inclusions. In: Samson IM, Anderson AJ, Marshall DD (eds). *Fluid inclusions: analysis and interpretation*. Mineralogical Association of Canada 32:213–232
- Bodnar R (1993) Revised equation and table for determining the freezing point depression of H₂O–NaCl solutions. *Geochim Cosmochim Acta* 57:683–684
- Bodnar R, Vityk MO (1994) Interpretation of microthermometric data for H₂O–NaCl fluid inclusions. In: De Vivo B, Frezzotti ML (eds). *Virginia Tech, Blacksburg, Fluid inclusions in minerals, methods and applications*, pp.117–130
- Bodnar RJ, Reynolds TJ, Kuehn CA (1985) Fluid inclusion systematics in epithermal systems. In: Berger BR, Bethke P (eds) *Reviews in Economic Geology*, 2nd edn., pp 73–97
- Boullier AM, Firdaus K, Robert F (1998) On the significance of aqueous fluid inclusions in gold-bearing quartz vein deposits from the southeastern Abitibi Subprovince (Quebec, Canada). *Econ Geol* 93:216–223
- Bowers TS, Helgeson HC (1983) Calculation of the thermodynamic and geochemical consequences of nonideal mixing in the system H₂O–CO₂–NaCl on phase relations in geologic systems; metamorphic equilibria at high pressures and temperatures. *Am Mineral* 68:1059–1075
- Campiglio C, Batholite de Bourlamaque (1977) *Service des gîtes minéraux, Etude ES-26.*, p 211
- Card K (1990) A review of the Superior Province of the Canadian Shield, a product of Archean accretion. *Precambrian Res* 48:99–156
- Chace FM (1956) Abbreviations in field and mine geological mapping. *Econ Geol* 51:712–723
- Chi GX, Guha J, Riverin G, and Trudel F (1992) Examination of an enigmatic flat gold-bearing quartz vein deposit in the Abitibi greenstone belt: a fluid inclusion approach (abs). *Pan-American Current Research on Fluid Inclusions 4th biennial conference*, Lake Arrowhead, CA, pp 23.
- Chiaradia M, Schaltegger U, Spikings R, Wotzlaw JF, Ovtcharova M (2013) How accurately can we date the duration of magmatic-hydrothermal events in porphyry systems? - An invited paper. *Econ Geol* 108:565–584
- Chown E, Harrap R, Moukhsil A (2002) The role of granitic intrusions in the evolution of the Abitibi belt, Canada. *Precambrian Res* 115:291–310
- Clauoué-Long JC, King RW, Kerrich R (1990) Archean hydrothermal zircon in the Abitibi Greenstone Belt: constraints on the timing of gold mineralisation. *Earth Planetary Sci Lett* 98:109–128
- Corfu F, Krogh TE, Kwok YY, Jensen LS (1989) U–Pb zircon geochronology in the southwestern Abitibi greenstone belt, Superior Province. *Canadian J Earth Sci* 26:1747–1763
- Couture JF, Pilote P, Machado N, Desrochers JP (1994) Timing of gold mineralization in the Val-d'Or District, southern Abitibi Belt; evidence for two distinct mineralizing events. *Econ Geol* 89:1542–1551
- Daigneault R, Mueller W, Chown E (2002) Oblique Archean subduction: accretion and exhumation of an oceanic arc during dextral transpression, Southern Volcanic Zone, Abitibi Subprovince Canada. *Precambrian Res* 115:261–290
- Davis DW, Lowenstein TK, Spencer RJ (1990) Melting behavior of fluid inclusions in laboratory-grown halite crystals in the systems NaCl–H₂O, NaCl–KCl–H₂O, NaCl–MgCl₂–H₂O, and NaCl–CaCl₂–H₂O. *Geochim Cosmochim Acta* 54:591–601
- De La Roche H, Leterrier J, Grandclaudé P, Marchal M (1980) A classification of volcanic and plutonic rocks using R1R2-diagram and major element analyses - its relationships with current nomenclature. *Chem Geol* 29:183–210
- Desrochers JP, Hubert C (1996) Structural evolution and early accretion of the Archean Malartic Composite Block, southern Abitibi greenstone belt, Quebec, Canada. *Canadian J Earth Sci* 33:1556–1569
- Desrochers JP, Hubert C, Ludden JN, Pilote P (1993) Accretion of Archean oceanic plateau fragments in the Abitibi, greenstone belt, Canada. *Geology* 21:451–454
- Diamond LW (1992) Stability of CO₂ clathrate hydrate + CO₂ liquid + CO₂ vapour + aqueous KCl–NaCl solutions: experimental determination and application to salinity estimates of fluid inclusions. *Geochim Cosmochim Acta* 56:273–280
- Diamond LW, Tarantola A, Stunitz H, Modification of fluid inclusions in quartz by deviatoric stress (2010) II: experimentally induced changes in inclusion volume and composition. *Contrib Mineral Petrol* 160:845–864
- Dimroth E, Imreh L, Rocheleau M, Goulet N, Evolution of the south-central part of the Archean Abitibi Belt (1982) Quebec Part I: stratigraphy and paleogeographic model. *Canadian J Earth Sci* 19:1729–1758
- Dimroth E, Imreh L, Goulet N, Rocheleau M, Evolution of the south-central segment of the Archean Abitibi Belt (1983) Quebec Part II: Tectonic evolution and geomechanical model. *Canadian J Earth Sci* 20:1355–1373
- Duan Z, Møller N, Weare JH (1992a) An equation of state for the CH₄–CO₂–H₂O system: I. Pure systems from 0 to 1000° C and 0 to 8000 bar. *Geochim Cosmochim Acta* 56:2605–2617
- Dubé B, Gosselin P (2007) Greenstone-hosted quartz-carbonate vein deposits. *Mineral deposits of Canada: a synthesis of major deposit types, district metallogeny, the evolution of geological provinces, and exploration methods*. Geological Association of Canada, Mineral Deposits Division. *Special Publication* 5:49–73
- Feng R, Kerrich R (1991) Single zircon age constraints on the tectonic juxtaposition of the Archean Abitibi belt and Pontiac subprovince, Quebec, Canada. *Geochim Cosmochim Acta* 55:3437–3441
- Feng R, Kerrich R (1992) Geochemical evolution of granitoids from the Archean Abitibi southern volcanic zone and the Pontiac subprovince, Superior province, Canada: implications to tectonic history and source regions. *Chem Geol* 98:23–70
- Feng R, Kerrich R, McBride S, Farrar E (1992) ⁴⁰Ar/³⁹Ar age constraints on the thermal history of the Archean Abitibi greenstone belt and the Pontiac Subprovince: implications for terrane collision, differential uplift, and overprinting of gold deposits. *Canadian J Earth Sci* 29:1389–1411
- Firdaus K (1995) *Etude des inclusions fluides dans une zone sismogénique fossile: les gisements aurifères mésothermaux Archéens de Val d'Or, Abitibi*. Unpublished Institut National Polytechnique de Lorraine, Québec, p 332 pp
- Frape S, Fritz P (1987) Geochemical trends for groundwaters from the Canadian Shield. In: Fritz P, Frape SK (Eds.) *Saline water and gases in crystalline rocks* Geological Association of Canada 33:19–38
- Frape S, Fritz P, McNutt RH (1984) Water-rock interaction and chemistry of groundwaters from the Canadian Shield. *Geochim Cosmochim Acta* 48:1617–1627
- Garofalo PS, Mass transfer during gold precipitation within a vertically extensive vein network (Sigma deposit - Abitibi greestone belt - Canada) (2004a) Part I Patterns of hydrothermal alteration haloes. *European J Mineral* 16:753–760
- Garofalo PS, Mass transfer during gold precipitation within a vertically extensive vein network (Sigma deposit–Abitibi greenstone belt–Canada) (2004b) Part II Mass transfer calculations. *European J Mineral* 16:761–776

- Goldfarb R, Baker T, Dube B, Groves DI, Hart CJR, Gosselin P (2005) Distribution, character and genesis of gold deposits in metamorphic terranes. In *Economic Geology 100th Anniversary Volume*:407–450
- Goldstein RH, Reynolds TJ (1994): Systematics of fluid inclusions in diagenetic minerals. *Society of Economic Paleontologists and Mineralogists, Short Course 31*, 199 pp.
- Goulet N (1978) Stratigraphy and structural relationships across the Cadillac - Larder Lake fault, Rouyn-Beauchastel area, Quebec. Ph.D. thesis, Queen's University, Kingston, Ontario. 155 pp.
- Groves DI, Goldfarb RJ, Gebre-Mariam M, Hagemann S, Robert F (1998) Orogenic gold deposits: a proposed classification in the context of their crustal distribution and relationship to other gold deposit types. *Ore Geol Rev* 13:7–27
- Groves DI, Goldfarb RJ, Robert F, Hart CJR (2003) Gold deposits in metamorphic belts: overview of current understanding, outstanding problems, future research, and exploration significance. *Econ Geol* 98:1–29
- Hanes J, Archibald D, Hodgson C, Robert F (1992) Dating of Archean auriferous quartz vein deposits in the Abitibi greenstone belt, Canada; $^{40}\text{Ar}/^{39}\text{Ar}$ evidence for a 70- to 100-my-time gap between plutonism-metamorphism and mineralization. *Econ Geol* 87:1849–1861
- Harrison TM, Fitzgerald JD (1986) Exsolution in hornblende and its consequences for $^{40}\text{Ar}/^{39}\text{Ar}$ age spectra and closure temperatures. *Geochim Cosmochim Acta* 50:2447–2453
- Harrison TM, Duncan I, McDougall I (1985) Diffusion of ^{40}Ar in biotite: temperature, pressure and compositional effects. *Geochim Cosmochim Acta* 45:2513–2517
- Hubert C, Trudel P, Gtlinas L (1984) Archean wrench fault tectonics and structural evolution of the Blake River Group, Abitibi Belt, Quebec. *Canadian J Earth Sci* 21:1024–1032
- Imreh L (1984) Sillon de Lamothe-Vassan et son avant-pays méridional: synthèse volcanologique, lithostratigraphique et géologique. Ministère de l'Énergie et des Ressources du Québec, MM 82–04:1–72
- Jébrak M, LeQuentrec MF, Mareschal JC, Blais D (1991) A gravity survey across the Bourlamaque massif, southeastern Abitibi greenstone belt, Québec, Canada: the relationship between the geometry of tonalite plutons and associated gold mineralization. *Precambrian Res* 50:261–268
- Jemielita R, Davis D, Krogh T (1990) U-Pb evidence for Abitibi gold mineralization postdating greenstone magmatism and metamorphism. *Nature* 346:831–834
- Jensen LS, Langford FF (1985) Geology and petrogenesis of the Archean Abitibi Belt in the Kirkland Lake area, Ontario. *Ont Geol Surv Misc Paper* 123:1–130
- Jolly WT (1978) Metamorphic history of the Archean Abitibi belt, metamorphism in the Canadian Shield. *Geological Surv Canada* 78–10:63–78
- Kerrick R, Kamineni D (1988) Characteristics and chronology of fracture—fluid infiltration in the Archean, Eye Dashwa Lakes pluton, Superior Province: evidence from H, C, O-isotopes and fluid inclusions. *Contrib Mineral Petrol* 99:430–445
- Kerrick R, King R (1993) Hydrothermal zircon and baddeleyite in Val-d'Or Archean mesothermal gold deposits: characteristics, compositions, and fluid-inclusion properties, with implications for timing of primary gold mineralization. *Canadian J Earth Sci* 30:2334–2351
- Kerrick R, Kyser TK (1994) 100 Ma timing paradox of Archean gold, Abitibi greenstone belt (Canada): new evidence from U-Pb and Pb-Pb evaporation ages of hydrothermal zircons. *Geology* 22:1131–1134
- Knight C, Bodnar R (1989) Synthetic fluid inclusions: IX. Critical PVTX properties of NaCl-H₂O solutions. *Geochim Cosmochim Acta* 53:3–8
- Kouzmanov K, Bailly L, Ramboz C, Rouer O, Beny JM (2002) Morphology, origin and infrared microthermometry of fluid inclusions in pyrite from the Radka epithermal copper deposit, Srednogie zone, Bulgaria. *Miner Deposita* 37:599–613
- Kretz R (1983) Symbols for rock-forming minerals. *Am Mineral* 68:277–279
- Kyser T, Kerrich R, *Geochemistry of fluids in tectonically active crustal regions* (1990) Short Course on Fluids in Tectonically Active Regimes of the Continental Crust. Mineral Assoc Canada 18:133–230
- Latulippe M (1966) The relationship of mineralization to Precambrian stratigraphy in the Matagami Lake and Val d'Or districts of Quebec. *Geological Assoc Canada* 3:21–42
- Lemarchand J, Tremblay A, Gobeil C (2010) Caractérisation et datation $^{40}\text{Ar}/^{39}\text{Ar}$ des structures aurifères de la région de Val d'Or, Abitibi. *Divex SC34*:1-12
- Lemarchand J (2012) Les minéralisations filoniennes aurifères du pluton de Bourlamaque (Val d'Or, Abitibi): synthèse structurale et apports de la datation $^{40}\text{Ar}/^{39}\text{Ar}$. Ph.D Thesis, Université du Québec à Montréal (UQAM) and Rennes University, 248 pp.
- Ludden J, Hubert C, Gariépy C (1986) The tectonic evolution of the Abitibi greenstone belt of Canada. *Geological Mag* 123:153–166
- Lydon JW (2007) An overview of the economic and geological contexts of Canada's major mineral deposit types. *Mineral deposits of Canada: a synthesis of major deposit-types, district metallogeny, the evolution of geological provinces, and exploration methods*. Geological Assoc Canada 5:3–48
- McCuaig TC, Kerrich R (1998) P-T-t-deformation-fluid characteristics of lode gold deposits: evidence from alteration systematics. *Ore Geol Rev* 12:381–453
- Mercier-Langevin P, Houllé MG, Dubé B, Monecke T, Hannington MD, Gibson HL, Goutier J (2012) A special issue on archean magmatism, volcanism, and ore deposits: part 1. Komatiite-associated Ni-Cu-(PGE) sulfide and greenstone-hosted Au deposits preface. *Econ Geol* 107:745–753
- Morasse S (1998) Geology, Structure and Timing of Gold Mineralization at the Kiena Deposit, Val D'Or, Québec. Ph. D. Thesis. Queen's University, Kingston, Ontario, p 362 pp
- Moritz RP, Crockett JH (1990) Mechanics of formation of the gold-bearing quartz-fuchsite vein at the Dome mine, Timmins area, Ontario. *Canadian J Earth Sci* 27:1609–1620
- Mulja T (1995) Magmatic and hydrothermal processes in rare-element granite-pegmatite systems: the Preissac-Lacorne batholith, Quebec, McGill University, p 370 pp, Ph. D. thesis Unpublished
- Neumayr P, Hagemann S, Banks D, Yardley BWD, Couture JF, Landis G, Rye R (2007) Fluid chemistry and evolution of hydrothermal fluids in an Archean transcrustal fault zone network: the case of the Cadillac Tectonic Zone, Abitibi greenstone belt, Canada. *Canadian J Earth Sci* 44:745–773
- Neumayr P, Hagemann SG (2002) Hydrothermal fluid evolution within the Cadillac Tectonic Zone, Abitibi Greenstone Belt, Canada: relationship to auriferous fluids in adjacent second- and third-order shear zones. *Econ Geol* 97:1203–1225
- Oakes CS, Bodnar RJ, Simonson JM (1990) The system NaCl-CaCl₂-H₂O: I. The ice liquidus at 1 atm total pressure. *Geochim Cosmochim Acta* 54:603–610
- Olivo GR, Chang F, Kyser TK (2006) Formation of the auriferous and barren North Dipper Veins in the Sigma Mine, Val d'Or, Canada: constraints from structural, mineralogical, fluid inclusion, and isotopic data. *Econ Geol* 101:607–631
- Olivo GR, Isnard H, Williams-Jones AE, Gariépy C (2007) Pb isotope compositions of pyrite from the C quartz-tourmaline vein of the Siscoe gold deposit, Val-d'Or, Québec: constraints on the origin and age of the gold mineralization. *Econ Geol* 102:137–146
- Olivo GR, Williams-Jones AE (2002) Genesis of the auriferous C quartz-tourmaline vein of the Siscoe mine, Val d'Or district, Abitibi subprovince, Canada: structural, mineralogical and fluid inclusion constraints. *Econ Geol* 97:929–947
- Pêcher A, Boullier AM (1984) Evolution à pression et température élevées d'inclusions fluides dans un quartz synthétique. *Bulletin de minéralogie* 107:139–153

- Pokrovski GS, Akinfiev NN, Borisova AY, Zotov AV, Kouzmanov K (2014) Gold speciation and transport in geological fluids: insights from experiments and physical-chemical modeling. In: Garofalo P, Ripley E (eds) Gold-transporting fluids in the Earth's crust, 402nd edn. Geological Society, Special Publication, London, pp 9–70
- Ramboz C, Pichavant M, Weisbrod A, Fluid immiscibility in natural processes: use and misuse of fluid inclusion data: II (1982) Interpretation of fluid inclusion data in terms of immiscibility. *Chemical Geology* 37:29–48
- Rive M, Pintson H, Ludden JH (1990) Characteristics of late Archean plutonic rocks from the Abitibi and Pontiac Subprovinces. In: Rive, M., Riverin, G., Simard, A., Lulin, J.M., Gagnon, Y. (Eds.), Les ceintures polymétalliques du Nord-Ouest québécois, Institut canadien des mines et de la métallurgie 43:65–76
- Robert F (1989) Internal structure of the Cadillac tectonic zone southeast of Val d'Or, Abitibi greenstone belt, Quebec. *Canadian J Earth Sci* 26:2661–2675
- Robert F (1990) Structural setting and control of gold-quartz veins of the Val d'Or area, southeastern Abitibi subprovince. Gold and Base-Metal Mineralization in the Abitibi Subprovince, Canada, with Emphasis on the Quebec Segment. University of Western Australia. Short Course Notes 24:167–210
- Robert F (1994) Vein fields in gold districts: the example of Val-d'Or, southeastern Abitibi Subprovince. *Geological Surv Canada Curr Res* 1994C:295–302
- Robert F, Brown AC (1986a) Archean gold-bearing quartz veins at the Sigma Mine, Abitibi greenstone belt, Quebec; Part I, Geologic relations and formation of the vein system. *Econ Geol* 81:578–592
- Robert F, Brown AC (1986b) Archean gold-bearing quartz veins at the Sigma Mine, Abitibi greenstone belt, Quebec; Part II, Vein paragenesis and hydrothermal alteration. *Econ Geol* 81:593–616
- Robert F, Kelly WC (1987) Ore-forming fluids in Archean gold-bearing quartz veins at the Sigma Mine, Abitibi greenstone belt, Quebec, Canada. *Econ Geol* 82:1464–1482
- Robert F, Poulsen K (2001) Vein formation and deformation in greenstone gold deposits. *Rev Econ Geol* 14:111–155
- Robert F, Boullier AM, Firdaus K (1995) Gold-quartz veins in metamorphic terranes and their bearing on the role of fluids in faulting. *J Geophys Res* 100:12861–12879
- Robert F, Poulsen KH, Cassidy KF, Hodgson CJ (2005) Gold metallogeny of the Superior and Yilgarn cratons. *Economic Geology* 100th anniversary volume:1001–1034
- Roussy J (2003) Relations entre la distribution de l'or, la structure, la composition des veines et de l'altération hydrothermale à la mine Beaufor, Val d'Or, Abitibi. Thesis, Université de Laval, Québec, QC, Québec. M. Sc, p 328 pp
- Scott CR, Mueller WU, Pilote P (2002) Physical volcanology, stratigraphy, and lithochemistry of an Archean volcanic arc: evolution from plume-related volcanism to arc rifting of SE Abitibi Greenstone Belt, Val d'Or, Canada. *Precambrian Res* 115:223–260
- Shepherd TJ, Rankin AH, Alderton DHM (1985) A practical guide to fluid inclusion studies. Blackie & Son, Glasgow, p 239 pp
- Sibson RH, Robert F, Poulsen KH (1988) High-angle reverse faults, fluid-pressure cycling, and mesothermal gold-quartz deposits. *Geology* 16:551–555
- Steele-MacInnis M, Bodnar R, Naden J (2011) Numerical model to determine the composition of H₂O–NaCl–CaCl₂ fluid inclusions based on microthermometric and microanalytical data. *Geochim Cosmochim Acta* 75:21–40
- Stefánsson A, Seward TM (2004) Gold(I) complexing in aqueous sulphide solutions to 500°C at 500 bar. *Geochim Cosmochim Acta* 68:4121–4143
- Sterner SM, Bodnar RJ, Synthetic fluid inclusions in natural quartz (1984) I Compositional types synthesized and applications to experimental geochemistry. *Geochimica et Cosmochimica Acta* 48:2659–2668
- Tanner MF, Trudel P (1989) Bourlamaque Batholith and its gold potential, Val d'Or, Quebec. *Canadian Inst Mining Metallurgy Bull* 82:33–42
- Tarantola A, Diamond LW, Stünitz H (2010) Modification of fluid inclusions in quartz by deviatoric stress I: experimentally induced changes in inclusion shapes and microstructures. *Contrib Mineral Petrol* 160:825–843
- Tessier AC (1990) Structural evolution and host rock dilation during emplacement of gold-quartz veins at the Perron Deposit, Val d'Or, Québec. M.Sc. thesis, Queen's University, Kingston, Ontario. Unpublished, 223 pp.
- Vanko D, Bodnar R, Sterner S (1988) Synthetic fluid inclusions: VIII. Vapor-saturated halite solubility in part of the system NaCl–CaCl₂–H₂O, with application to fluid inclusions from oceanic hydrothermal systems. *Geochim Cosmochim Acta* 52:2451–2456
- Williams-Jones AE, Bowtell RJ, Migdisov AA (2009) Gold in solution. *Elements* 5:281–287
- Wong L, Davis D, Krogh T, Robert F (1991) U–Pb zircon and rutile chronology of Archean greenstone formation and gold mineralization in the Val d'Or region, Quebec. *Earth Planet Sci Lett* 104:325–336
- Zhang YG, Frantz JD (1987) Determination of the homogenization temperatures and densities of supercritical fluids in the system NaCl–KCl–CaCl₂–H₂O using synthetic fluid inclusions. *Chem Geol* 64:335–350
- Zweng PL, Mortensen JK, Dalrymple GB (1993) Thermochronology of the Camflo gold deposit, Malartic, Quebec; implications for magmatic underplating and the formation of gold-bearing quartz veins. *Econ Geol* 88:1700–1721